A New Generalized Philosophy and Theory for Rubber Friction and Wear

Y. Fukahori*, P. Gabriel, H. Liang and J.J.C. Busfield

School of Engineering and Materials Science, Queen Mary University of London, Mile End Road, London, E1 4NS, UK

Abstract

The authors propose a new philosophy and theory for rubber friction and wear that are significantly different from the existing classical theories. Several distinctive features of rubber friction such as the exceedingly high friction coefficient and the intense stick-slip motion during frictional sliding all result from the sticky surface behavior exhibited by a cross-linked rubber, where there is a meniscus force brought about at the interface between the rubber and the rigid surface. The total friction coefficient μ_{all} incorporates three factors including an adhesion term μ_{adh}, a deformation term μ_{def} and a crack formation term μ_{crac}. This generates an equation

$$\mu_{all} = \mu_{adh} + \mu_{def} + \mu_{crac} \fallingdotseq K_1 \eta V^m \left[1 + K_2 \left(\frac{\tan\delta}{\sqrt{2}} + \sqrt{2} K_\varepsilon c \right) E^{-7/6} W^{1/6} \right]$$

where η is the viscosity of the uncross-linked phase, E the modulus of the cross-linked phase, V sliding velocity, c crack length, W normal load, K_1, K_2, K_ε and m are all coefficients whose characteristics also govern rubber wear. The adhesion term is the most dominant factor during rubber friction, which roughly contributes about 70～80% of the total friction coefficient.

The close relationship between the observed stick-slip motion, abrasion pattern formation and wear have been verified experimentally. The abrasion pattern is initiated by the high frequency vibration and the steady abrasion pattern together with steady wear is promoted by the stick-slip motion. Steady wear rate $\dot{V}$ could be estimated theoretically as a function of the steady abrasion pattern distance D_{ab} using an equation $\dot{V} = k' D_{ab}^3$, which indicates that many of the characteristics observed in rubber wear are also fundamentally governed by the intense stick-slip motion induced by the sticky rubber surface.

Keywords

Rubber friction, interfacial properties, uncross-linked phase, cross-linked rubber, meniscus formation, stick-slip motion, rubber wear, crack initiation, abrasion pattern formation, steady wear rate

1. INTRODUCTION

Most of the accepted physical concepts and theories of rubber friction were initially established about half a century ago and they have been widely adopted to explain the friction and wear of rubber. The dominant theories for rubber friction that were initially developed by Schallamach[1]and were extended by Grosch [2], Ludema and Tabor [3]have been well summarized by Moore [4] in his textbook. These were all based on the assumption that frictional behavior of rubber significantly depends on the viscoelastic characteristics of rubber material as described for example using a WLF transformation [5]. Following this approach, a significant effort has been spent attempting to control tan δ of rubber materials in the research and developments of materials for applications such as tyres where the detailed nature of the rubber friction is important.

However, it is undoubtedly clear that the existing friction theories and concepts are unable to answer some remaining essential questions in rubber friction such as: (1) Why is the surface of a rubber exceedingly sticky when compared to a plastic with almost identical molecular structures? (2) Why is friction coefficient of rubber (which ranges typically from 1 to 3) significantly higher than that for metal and plastic materials where the magnitude is often lower than 0.5? (3) Why is the frictional sliding of rubber almost always accompanied with a jagged stick-slip motion, whereas other materials can slide much more smoothly without producing this type of violent stick-slip motion? It is quite natural to presume that the frictional behavior of a rubber might be influenced by the surface characteristics of the material and of course, the above fundamental questions all corelate closely with the specific surface characteristics of rubber. Nevertheless, the classical theories focus primarily on viscoelastic properties of the bulk rubber material and often ignore the interfacial problems of rubber.

The present paper firstly focuses on the surface characteristics of rubber whilst trying to understand the real features existing on the surface of cross-linked rubber, where is shown that the dominant factor encountered during rubber friction is the adhesion force caused by the meniscus formation in the interface between the uncross-linked phase in the cross-linked rubber and the solid surface. Based on this basic approach, the authors propose a new general and comprehensive philosophy for rubber friction, whilst answering all the above fundamental questions both theoretically and experimentally. Secondly, the present paper deals with rubber wear in the relation with abrasion pattern formation, where the very close relation between both phenomena is shown experimentally. The abrasion pattern is initiated by the high frequency vibration and the steady abrasion pattern is promoted by the stick-slip motion, thus accordingly it might be concluded that rubber wear is also fundamentally determined by the stick-slip motion originated by the sticky rubber surface.

2. BACKGROUND

2.1 Classical concepts and theory of rubber friction

Schallamach [1] was one of the earliest researchers to report that the frictional force of rubber

depends on both the temperature and the sliding velocity, where the frictional force increases slightly with increasing velocity and increases greatly as the temperature is reduced. An exponential relationship between the friction coefficient and temperature derived from his experiments is similar to the relationship between fluidity and temperature during the viscous flow of liquid. Schallamach introduced a molecular rate process based on an activation mechanism to explain why the surface of a rubber behaves like a liquid. In the rate process, molecules attach and detach to the substrate continuously so that rubber chain ends make small jumps in the sliding direction under a tangential stress, as is discussed in greater detail by Bartenev and El'kin [6].

Grosch [2] extended this work and prepared a much greater dataset that demonstrated the dependence of rubber friction on the sliding velocity and temperature, where the friction coefficient was measured at a low sliding velocity of 10^{-5} to 1 cm/s as a function of temperature. Grosch applied a WLF superposition concept [5] to these data to obtain an unique bell-shaped master curve between the friction coefficient and sliding velocity over a very wide range from 10^{-8} to 10^{8} cm/s at 20°C, as shown in Fig. 1. He assumed that a peak velocity in the master curve corresponds to a peak value of $\tan\delta$. Ludema and Tabor [3] also performed similar experiments and they also obtained a master curve using a similar WLF transform. Since these findings were reported, the concept that the friction behavior of rubber is governed by viscoelastic properties of rubber block itself has been widely accepted in the field of rubber research.

Following them, Moore [4] proposed a theory of rubber friction based on the concept that total friction coefficient μ_{all} can be derived by the summation of the adhesion term μ_{adh} and the deformation term μ_{def} based on a similar treatment in metals,

$$\mu_{all} = \mu_{adh} + \mu_{def} = K'_1 \left[\frac{E}{Pr} + K'_2 \left(\frac{P}{E}\right)^n\right] \tan\delta \quad (1)$$

$$\mu_{adh} = K'_1 \left(\frac{E}{Pr}\right) \tan\delta \quad (2)$$

$$\mu_{def} = \mu_{hys} = K'_3 \left(\frac{P}{E}\right)^n \tan\delta \quad (3)$$

where K'_1、K'_2、K'_3 are constant, E modulus and P normal pressure, $r \leqq 1$, $n \geqq 1$ and μ_{hys} corresponds to the amount of hysteresis energy lost during the deformation of a rubber component in contact with a rigid rough surface. The most intriguing feature of equation (1)～(3) is that μ_{all}, μ_{adh} and μ_{def} can all be represented as a function of typical materials constants, tan δ and E. As expected therefore, the velocity dependence of the friction coefficient has a peak at a glass transition temperature (velocity), as shown in Fig.1. Moore's theory backed up by Grosch's data has become the most basic concept of the rubber friction and it is still widely accepted.

2.2 Subsequent developments of the rubber friction

A quarter of a century on from Grosch's paper, Barquins and Roberts [7] repeated the Grosch experiments very carefully using a similar rubber compound under the same experimental conditions and they analyzed their data using the same WLF transform as Grosch, which produced the results shown in Fig.2. They pointed out that the friction coefficient increases gradually with increasing velocity up to a velocity of around 10^2 mm/s, above which it levels off until about 10^4 mm/s, which indicates that the friction coefficient of rubber does not change drastically to form a bell-shaped curve. They also indicated that over the velocity range from around 10^4mm/s, the sliding system becomes quite unstable when an intense stick-slip motion took place.

Very recently Tolpekina and Persson [8] obtained similar results to the data of Barquins and Roberts as shown in Fig. 3, where the friction coefficients were measured over a very wide velocity range with presumably using the WLF transform for three rubber compounds on the sliding conditions of both the dry and wet (in water) on a smooth glass surface. The coefficient of friction measured on the dry condition showed a gradual increase with an increasing velocity, which did not show the bell-shaped peak, being quite similar to the results that Barquins and Roberts obtained. Fig.3 also shows an interesting result that the friction coefficient measured in water was much smaller than that on the dry condition (discussed in detail later). Sakai [9] measured the friction coefficient of a typical rubber compound for a tyre tread as a function of sliding velocity continuously over a velocity range from 10^0 to 10^3 mm/s at a constant temperature without using the WLF transform, as shown in Fig. 4. At 30°C, for example, the friction coefficient increases with velocity up to around 10^2 mm/s and then it seems to level off towards 10^3 mm/s.

Although of course, it is not easy to speculate as to the cause of the discrepancy between Grosch report and the others reported here (Barquins and Roberts, Tolpekina and Persson and Sakai), also it is not yet certain whether a WLF formulation is generally applicable to the rubber friction even after more than half a century. Under such a situation in practice, it seems likely that using the Grosch method of measuring the data measured only at a low sliding velocity of less than 10 mm/s which is then scaled to cover a very wide velocity range from 10^{-7} to 10^9 mm/s produces a significant risk, in particular when we hope to optimize rubber friction at a high speed in excess of 100 km/h ($=3\times10^4$ mm/s).

It might be reasonable under such a situation to accept Sakai's report (Fig.4) as a realistic basic data set for rubber friction over a considerably high velocity region. Thus, together with the concept of Barquins and Roberts and Tolpekina and Persson, it can be concluded that at room temperature the friction coefficient of rubber may increase gradually and reach a flat plateau region at around 10^2～10^4 mm/s, and above this velocity range a sliding system becomes unstable and violent stick-slip motion occurs. In addition, if this conclusion is correct, then equations (1) and (2) determined from $\tan\delta$ may no longer be appropriate, because these equations were developed to match with Grosch's data to demonstrate the sharp bell-shaped peak corresponding to $\tan\delta$ around the glass transition

temperature (velocity) of the material. Thus, it might be necessary to propose a new philosophy and theory for the rubber friction to advance the classical theory, which is constructed based not on the material but on the interfacial behavior. Although of course, the works performed by Grosch, Moore and others gave a new epoch-making insight how to understand the rubber friction for the first time, it is also true that many unsolved phenomena have been left unanswered for many years concerning the rubber friction and wear in which the classical theories no longer work.

2.3 Recent reports to characterize the surface of cross-linked rubber

The experimental and theoretical consideration proposed by Johnson, Kendall and Roberts [10] are significant when trying to understand the characteristics of a rubber surface, where a contact area between rubber sphere and a flat rubber surface or between gelatin spheres are measured. They showed that a strong adhesive force exists between both surfaces, whose capacity increases the contact area to be much larger than that predicted by Hertzian contact around the zero normal load, as shown in Fig. 5. Both surfaces adhere suddenly when they approach each other and come off suddenly when they separate from each other in both cross-linked rubbers and gelatins. This instantaneous adhesion and separation at the interface are similar the formation and destruction of meniscus in a liquid sandwiched between two solid surfaces. Maugis [11] advanced the theory given by Johnson et al. using the Dugdale model [12] from fracture mechanics and suggested that the strong adhesive force might be resulted from a meniscus force. However, Johnson et al. and Maugis were unable to answer why such a meniscus should form on the surface of a cross-linked rubber.

There is another fundamental question that has remained unanswered for a long time, which is why the surface of a cross-linked rubber is considerably stickier when compared with plastic or other solids. Saeki [13] indicated the close relation between friction coefficient and stickiness, where the degree of stickiness (stickiness index) was measured by finger-tip test, as shown in Fig.6. The finger-tip test is a simple but quite useful method for direct judgement of the stickiness, where 19 researchers measured the stickiness of 14 rubber samples. As expected, Fig.6 shows that the stickiness that we simply feel with fingers roughly denotes the friction coefficient. Saeki also showed the relation between the stickiness and stick-slip motion, the higher the stickiness, the stick-slip motion occurs more intensely.

Fukahori [14] proposed a new structure model for vulcanized crosslinked rubber, in which cross-linked rubber does not consist of homogeneous cross-linked network structure of rubber molecules but a heterogeneously co-continuous structure of an uncross-linked phase and a cross-linked phase. In the model, the continuous cross-linked phase (approximately 70% of the volume) is surrounded by another continuous uncross-linked phase (30%), thus both phases make co-continuous structures, the phase separation being of the order of a few μm. Fukahori, Gabriel and Busfield [15] also pointed out that uncross-linked rubber before vulcanization includes many additives such as steric acid, oil, rosin and other chemicals that work as tackifiers in the uncross-linked rubber. This means that the surface

of the uncross-linked phase which has the same characteristic as the uncross-linked rubber may also be highly sticky, which might be useful for forming a meniscus at the interface more easily.

Nakajima et al. [16] measured the structure of vulcanized cross-linked rubber using AFM techniques and found the existence of heterogeneous structure of different modulus of the order of a few μm in vulcanized cross-linked rubber, where the hard phase seems to correspond to the cross-linked phase and a soft phase to the uncross-linked phase. In addition, they confirmed that adhesive energy of the hard phase was less than 0.1J/m^2, whereas that of the soft phase was 0.4 J/m^2. Their observation supported the structure model proposed by Fukahori and the highly sticky characteristics of the surface of the cross-linked rubber.

According to Schallamach [17], when a rigid slider slides over a rubber surface, ridges of rubber known as a wave of detachment (Schallamach waves) are formed, which cross over the contact zone on a rubber surface, Although Schallamach and Barquinsand and Courtel [18] indicated that the ridge in which air is trapped may be formed by buckling a protrusion of rubber, they could not explain how the buckling occurred in front of the slider. Fukahori, Gabriel and Busfield [15] proposed a new interpretation for the formation of Schallamach waves, by showing experimentally that such a buckling only occurred when a meniscus was formed just in the front of a slider at the beginning of stick stage during stick-slip movement.

Fukahori and Yamazaki [19,20] observed another essential feature of rubber friction when they studied the dynamic friction behavior of cross-linked rubber over a wide range of frequencies. When a rigid slider moves over a rubber surface, two kinds of vibration are generated, one being a stick-slip motion in a range of 1-20Hz, the second being vibrations with a much higher frequency in the range of 1000Hz, as shown in Fig. 7, where the regions I and II correspond to the stick and slip stage, respectively. The high frequency vibration corresponds to the natural resonance frequency of rubber induced during the slip stage of stick-slip motion. When a rigid slider detaches from the compressed rubber surface during the slip stage, the released rubber surface vibrates at a high frequency in a similar way that a guitar string vibrates after it has been plucked.

Fukahori and Yamazaki [19,20] also found another important phenomenon that numerous parallel microcracks are created on the surface of the rubber by the high frequency vibration even after just a single pass of a slider. Fig. 8 shows a NR surface after a single pass by a slider, the distance between microcracks being the same as the period of the high frequency vibration, and the microcracks thus initiated propagate to create the abrasion patterns. This means that a significant amount of frictional energy is dissipated associated with crack formation and propagation during the sliding of rubber, which finally manifests itself as the wearing of the rubber resulting in the formation of an abrasion pattern. Accordingly, it is clear that the energy for crack formation must be included in the rubber friction model and cannot be neglected from the total frictional force, as is discussed in greater detail later.

3. EXPERIMENTS and RESULTS

Two kinds of experiment and a simulation were performed in this work to elucidate a new and novel principle of rubber friction and to address the three fundamental questions presented in the introduction. Each experiment is explained separately with details of the experimental procedure and the results.

3.1 Vibration of high frequency and micro-crack formation during frictional sliding

The first experiment clarifies the real characteristics of stick-slip motion and the high frequency vibration in greater detail, where the experimental procedures to measure the vibrations are the same as the previous method adopted by Fukahori and Yamazaki [19], and which are explained in greater detail in the section **4.4.2**. A steel slider made from a razor blade, whose edge is a semi-circle, moves tangentially on a NR rubber block specimen with a sliding velocity 20mm/s at room temperature. The frictional force is measured using a strain gauge connected to the slider, and the high frequency vibration is monitored using an acceleration transducer bonded to the surface of the rubber block (see Fig.36). Typical spectra of stick-slip motion (upper) and high frequency vibration (lower) for several rubber compounds, unfilled and filled with HAF carbon black are shown in Fig. 9 and Fig. 10, where NR1 and SiR1 (unfilled), NR2, SBR2 and BR2 (20phr filled) and NR3 (50phr filled), measured at a normal load of 30N and a sliding velocity of 20 mm/s. As observed in the figures, intense stick-slip motions together with violent high frequency vibrations occur under almost all sliding conditions for all rubber compounds, which of course results from the high stickiness of the rubber surface.

In general, although stick-slip motion is regarded as a horizontal alteration of stop (stick) and slide (slip), but simultaneously, another dynamic motion of the slider occurs. That is, the vertical position of slider changes periodically together with the horizontal movement of slider, moving upwards in the slip stage and downwards during the stick stage as shown schematically in Fig. 11. Fig. 12 shows the relation between the stick-slip distance $d_{s\text{-}s}$ calculated from the force versus time curve (Fig.7, Fig.9 and Fig.10) and the depth of the indentation of the slider into the rubber surface d_{ind} measured using an optical microscope, where it is shown that both the distances are almost equal. It is clear that the stick-slip motion is related closely to the adhesive characteristic of the surface of the rubber, which can be understood easily by comparison with the situation when a pencil is made to slide on an adhesive tape, where the pencil does not slide smoothly but jumps with intense skipping (stick-slip motion). If the stickiness of the tape is increased, then a longer skipping distance results. Fig. 13 shows the relationship between $d_{s\text{-}s}$ and the modulus of the rubber E and between $d_{s\text{-}s}$ and normal load W, where there is an almost linear relation between $d_{s\text{-}s}$ and $1/\sqrt{E}$ and between $d_{s\text{-}s}$ and $\sqrt{W}$. In addition, Fig. 14 shows a linear relationship between $d_{s\text{-}s}$ and $\mu/\sqrt{E}$, where μ is the friction coefficient. Thus it is also clear that $d_{s\text{-}s}$ is proportional to μ. Therefore, it can be written from these relations as $d_{s\text{-}s} = k_1 \mu (W/E)^{1/2}$, where k_1 is a coefficient.

Fig. 13 and Fig. 14 illustrate that a sticky rubber surface, which is reflected because it has a high μ together with low modulus, produces an intense displacement of the slider in both the horizontal and vertical directions during stick-slip motion. This generates a significant stress in tension and compression at the edge of slider. This behavior is known as ploughing in rubber friction. This generates a significant stress concentration which initiates crack formation and propagation and finally results in the wearing of the rubber. In general, although the hysteresis energy loss is dissipated during the contact between the rubber surface and the irregular rigid surface, it may be appropriate to suggest that the most significant energy dissipation occurs during these repeated large dynamic movements during stick-slip motion. Thus, we can conclude that the adhesion term is the first basic element when determining the rubber friction, whose magnitude influences all the other terms in the friction system. To explain this more clearly, consider that the adhesive characteristic of the rubber surface determines the basic friction coefficient as well as the intensity of the stick-slip motion, which finally determines the magnitude of deformation and any resulting wear and crack formation.

The next set of experiments explored the high frequency vibration associated with stick-slip sliding that produces numerous microcracks on the surface of the rubber even during a single frictional pass as shown in Fig.8. The left-hand figure in Fig. 15 shows the process where a slider begins to slide at a position at the top A and reaches the bottom C passing through the intermediate B on a NR block of 120mm length. The vertical vibration of high frequency is monitored continuously with an acceleration transducer (AT) bonded to the rubber surface near to point B slightly apart from the sliding path of the slider. The right-hand figure in Fig. 15 shows the spectra of the vibration at the high frequency monitored by the acceleration transducer at point B throughout the entire sliding process from A to C, where the surface of the rubber vibrates vertically. In the spectra, many kinds of vibration with a much higher frequency are included, being a fundamental wave of 600Hz and its harmonic waves. The higher order harmonic waves disappear at a long distance from point B due to the energy dissipation of the rubber.

The phenomena observed in Fig. 15 indicates that a vibration with a high frequency is initiated at the front edge of slider, but once the vibration starts, it does not disappear even momentarily, but it spreads and covers all the rubber surface surrounding the slider. In such a situation the edge of the slider will bounce over the top of the vibrating wavy rubber surface, which creates periodic cracks at the collision points, being similar to the situation that arises when a boat moves forwards over a wave. Not surprisingly, the distance between microcracks agrees well with the period of vibration at a high frequency, as shown schematically in Fig. 16.

3.2 Effects of slider edge sharpness on the friction coefficient

The second experiment focused on the question of how the sharpness of the edge of the slider influences the friction coefficient. In this experiment sharp cone shaped sliders with an edge angle

ranging between of 10° and 120° were slid on a flat SBR surface with a sliding velocity of 0.1mm/s at room temperature. Fig. 17 shows the stick-slip motion generated when using four different types of cone sliders, indicating that the sharper the cone angle, the greater the intensity of the stick-slip motion with a greater amplitude and a larger stick-slip distance. On the rubber surface, a lot of visible macro-cracks of mm order were observed even after a single pass, the sharper the cone angle, the larger the distance between these cracks and the deeper their depth. Fig. 18 shows the distance between cracks (d_{crac}) against normal load, where is seen that the distance is not much different for all the various edge angles when a normal load is very small, but the difference increases gradually as normal load increases, the smaller the cone angle, the distance increases more rapidly.

Fig. 19 shows the relation between the friction coefficient and normal load for cone sliders, where although the friction coefficient is hardly affected by the sharpness of the cone when the load is very small, it increases greatly as the load increases, the sharper the edge of cone, more rapidly the friction coefficient increases. When the angle is smaller than 30°, the normal load dependence of the friction coefficient shows a positive slope in the μ versus load relationship, which can be explained by assuming that a sharp cone cuts into the surface of the rubber which produces an anchoring effect. This anchoring effect seems to induce much larger effect than the original stickiness of the surface for generating an adhesive force, which gives rise to a greatly increased friction coefficient under a heavy loading condition, just like a needle puncturing a tyre. In general, when a rubber surface contacts with a slider with a smooth surface, the abrasion pattern grown from microcracks that are induced by the high frequency vibrations as indicated in Fig. 8 and Fig.16 propagate gradually into macrocracks (and then form an abrasion pattern). However, in contact with a slider with a sharp edge, the cracking may skip over an initial stage of microcrack formation directly to an abrasive macrocrack even after just a single contact, thus the distance $d_{s\text{-}s}$ becomes equal to the distance d_{crac}

Fig. 20 shows that the distance between macro-cracks d_{crac} is almost equal to the stick-slip distance $d_{s\text{-}s}$ when sharp cones are used, where the friction coefficient is also plotted against $d_{s\text{-}s}$, thus clearly indicating that $d_{s\text{-}s}$ is proportional to the friction coefficient μ . This is the same relationship as observed in Fig. 13 and Fig. 14 when a blade with semi-circular edge was used, showing that the adhesive friction force might incorporate an anchoring effect into any sliding system model, whose intensity decides the magnitude of stick-slip motion. This means, in other words, that the meniscus formed on the uncross-linked phase also works as the anchoring effect between the surface of rubber and the rigid solid (see Fig. 26 and Fig. 29), when it generates a strong adhesive frictional force. The stick-slip motion thus induced decides in turn the extent of the rubber deformation together with the material hysteresis loss, and simultaneously it decides the rate of crack formation and propagation resulting in the rate of wear, which is discussed in more detail later.

3.3 FEA simulation to separate the adhesion and deformation term

Finally, FEA simulations were used to investigate whether the adhesion term and the deformation term in frictional force are separable or not. All the finite element models were performed using the explicit dynamics finite element package ABAQUS/Explicit, version 6.4, which works well with models up to very large deformations and where complicated contact is encountered. Fig. 21 shows the simulation model for frictional sliding of SBR used in the previous paper [21], where a slider passes over a ridge made like the geometry of an abrasion pattern, where the slider initially moves down vertically to compress the rubber surface (a) and moves horizontally until it completely passes over the ridge (b) and finally returns to the initial geometry after a buckling of the ridge.

In the simulation the horizontal force is calculated as a function of the adhesion friction coefficient μ_{adh} during a whole sliding process of the slider. The total tangential frictional force F_{all} generated in this process consists of both the contributions from the adhesion term and the deformation term. For example, for the case $\mu_{adh} = 0$, as shown in Fig. 22, the total horizontal force F_{all} is zero before the ridge is encountered, but then it increases gradually and comes up to a peak maximum value caused by the maximum deformation of the ridge and drops off again after relaxation. In this case, the maximum peak value F_{all} purely corresponds to the contribution from the deformation term, where the negative values shown in Fig. 22 result from a buckling instability in the snap through part of the calculation.

Since the total frictional force F_{all} derived from the peak value in other cases of the finite μ_{adh} value includes both an adhesion frictional force F_{adh} and a deformational frictional force F_{def}, and accordingly, F_{def} can be calculated by deducting F_{adh} (given by the flat region in Fig. 22) from the total peak value F_{all}, as $F_{def} = F_{all} - F_{adh}$. In Fig. 23, the adhesion term F_{adh} and the deformation term F_{def} are plotted separately as a function of μ_{adh}. Naturally, although F_{adh} increases proportionally with μ_{adh}, F_{def} is almost constant regardless of a different magnitude of μ_{adh}. This means that the deformation frictional force could only be decided by the maximum deformation of a rubber unit, independent of the adhesive character of the system. However as shown in Fig. 13, Fig. 14 and Fig. 20, since the dimensions of the deformation are decided by the magnitude of stick-slip distance $d_{s\text{-}s}$ and hence by the adhesive characteristics of rubber, the deformation term also depends on the adhesive friction coefficient, thus indicating that both the terms F_{def} and F_{adh} and also the crack formation term F_{crac} are all inseparable from each other. Of course, since the magnitude of μ_{adh} is in the range of 1～3, F_{adh} might substantially be much larger than F_{def} in Fig. 23 for rubber friction. This is discussed in greater detail later.

4. DISCUSSION

4.1 Characterization of the surface of cross-linked rubber

It might be of significance to the fundamental understanding of rubber friction to answer the question as to why the surface of a rubber is so sticky, because undoubtedly several specific characteristics of the rubber friction relate to the sticky surface as shown in Fig.6. In particular, it may

be a key point when trying to understand why there is such a big difference in friction coefficient between rubber (1～3) and plastic (less than 0.5 [22]), despite both materials having almost identical molecular structures. Roberts and Thomas [23] measured an adhesive energy ($\Delta\gamma$) between vulcanized cross-linked rubbers plotted against peeling velocity in a peeling test that used a glass cylinder rolling on a plane rubber track of NR and Polychloroprene at 25°C, as shown in Fig. 24. The adhesive energy between cross-linked rubber and glass increases gradually with increasing velocity. This behavior is similar to the velocity dependence of the frictional force of a cross-linked rubber as shown in Fig.4 and it is also similar to the velocity dependence of a liquid, where the viscosity increases with increasing velocity. Of course, such a strong adhesive peeling force is not present on the surface of a plastic material, which suggests that the surface of a cross-linked rubber is covered by a liquid like material, which generates a sticky feeling on the surface and yields a very high friction coefficient for a cross-linked rubber.

What is the origin of this liquid-like material on the surface of an apparently crosslinked rubber which can yield such a strong adhesive force? According to the JKR experiment [10] shown in Fig.5, cross-linked rubbers join together each other very suddenly when they are brought into contact and separate also very suddenly from each other when pulled apart. This behavior is likely to result from the highly sticky and adhesive characteristic of the surface of the cross-linked rubber, which might result from meniscus formation on the rubber surface, as Maugis [11] suggested and Fukahori, Gabriel and Busfield [15] showed experimentally. One could argue that the softness of rubber makes the real contact area much larger, which produces a much higher friction coefficient than for say a plastic, however this does not explain the behavior at a very small deformation, in particular, at a zero normal load in the JKR experiment, where it is just indicated that the adhesive energy is independent of the modulus of rubber. In addition, the JKR experiment also indicated that gelatin behaves just like cross-linked rubber, which supports the idea of meniscus formation on the surface of cross-linked rubber, because the surface of gelatin is always covered with liquid, which immediately creates the meniscus.

Thus, the next question to be addressed is why and how the meniscus is formed on the surface of cross-linked rubber. According to the structure model for vulcanized crosslinked rubber proposed by Fukahori [14], vulcanized cross-linked rubber consists of heterogeneously co-continuous structures of a cross-linked phase (approximately 70% in volume) and an uncross-linked phase (30%), being separated from each other at a length scale of a few μm. Fig. 25 is a schematic image model for the surface of a cross-linked rubber, where the black and white areas correspond to the cross-linked phase and uncross-linked phase, respectively. Although the uncross-linked phase occupies a smaller proportion of the surface area, it is set up over the surface like a network structure and its highly viscous characteristic introduces a much greater adhesive force than the van der Waals force on the surface of the cross-linked phase and the plastic. Similar structures were also observed in a gel using an AFM technique by Suzuki, Yamazaki and Kobiki [24], where the irregularity of a solid phase of

the order of a few micrometers were spread over the surface of the gel and a liquid phase filled the gaps surrounding the solid phases.

Here we just have a comment concerning the structural stability of Fig. 25, because it might be asked whether the uncross-linked materials flow out or bleed from the rubber surface continuously, resulting in the unstable material state. We can say, however, that this is unlikely, because the viscosity of the uncross-linked rubber molecule with a very high molecular weight is high, and in addition it forms a thin capillary tube surrounded by the cross-linked phase as shown in Fig. 25, whose diameter may be 0.1～1μm order. Thus accordingly, the uncross-linked rubber might not flow out from such the thin tube, resulting in the stable structural condition of the uncross-linked phase and the cross-linked phase in the cross-linked rubber.

In practice, the surface of an uncross-linked rubber after extrusion and sheeting is quite sticky, which when pressed together results in both surfaces adhering to each other instantaneously and they cannot be separated again. Many rubber additives are blended as tacky adhesives into the uncross-linked rubber, some of them bloom and create a highly viscous liquid on the surface of uncross-linked rubber. Therefore, if the surface of the uncross-linked phase has the same characteristic as the original uncross-linked rubber, then such viscous liquid-like additives might form a meniscus at the interface between the rubber and the solid. Fig. 26 shows schematically the proposed meniscus formation by the uncross-linked phase and the van der Waals contact by the crosslinked phase when the cross-linked rubber is brought into contact with a solid surface.

Concerning the meniscus formation as commented in Fig.3, Tolpekina and Persson [8] measured friction coefficient as a function of velocity on the sliding condition of both a dry contact and a wet contact on a smooth glass surface. Although the friction coefficient measured on the dry contact is quite similar to the results measured by Barquins and Roberts (Fig.2), the friction coefficient measured in the water is much smaller, almost 1/5～1/3 of that given by the dry condition as shown in Fig.3. They measured separately an interaction force (adhesion work) between rubber surface and glass ball, in which the adhesion work in the water is almost one tenth of that of the dry contact. Both the results, of course, indicate that the water at the interface greatly inhibits the meniscus formation by the uncross-linked rubber phase. In other words, the very high friction coefficient of the cross-linked rubber compared with the plastic whose friction coefficient is less than 0.5 is obviously a result from the meniscus formation in the interface.

4.2 Proposal of new theoretical equations for rubber friction

4.2.1 Adhesion term in the updated rubber friction model

The total dynamic frictional force of rubber F_{all} consists of the adhesion term F_{adh} and the stick-slip motion term $F_{s\text{-}s}$,

$$F_{all} = F_{adh} + F_{s\text{-}s} \tag{4}$$

Furthermore, since the stick-slip motion generates both a deformation of the rubber component and crack formation on the rubber surface, the stick-slip motion term is divided into a deformation term with hysteresis loss F_{def} and a crack formation term F_{crac},

$$F_{s\text{-}s} = F_{def} + F_{crac} \quad (5)$$

The adhesive force on the contact surface is assumed to consist of the summation of the meniscus force formed on the uncross-linked phase and the van der Waals force on the cross-linked phase. However, since the contribution from the van der Waals force is relatively small compared with the meniscus force, it can be neglected except for the case when there is a very large normal pressure as is discussed later, and thus the adhesive force results principally from the meniscus force only.

According to Bowden and Tabor [25], the meniscus force F_m is given as the product of the Laplace force and the area over which the Laplace force works, which is represented by equation (6) under a static condition as shown schematically in Fig. 27,

$$F_m = 4\pi R\gamma \quad (6)$$

where R is the radius of the sphere and γ is the surface tension of the liquid. They also gave the meniscus force under dynamic conditions, that arises when the meniscus formed under the static condition is separated by force F from the distance h_1 to h_2, the time for separation t is given as,

$$t = \frac{3\pi\eta R^4}{4F\left(\frac{1}{h_1^2} - \frac{1}{h_2^2}\right)} \quad (7)$$

where η is viscosity of the liquid. By exchanging $1 / t$ with shear velocity V and setting a meniscus area as A_m, the meniscus force F_m which is the adhesive force F_{adh} is seen to be a function of velocity V, where K_1 is a constant.

$$F_{adh} = F_m = K_1 \eta A_m V \quad (8)$$

In addition, by introducing the assumption that the meniscus area A_m increases proportionally with normal load W, as is the case when the yielded area increases proportionally with normal load in metal, then the adhesive friction coefficient μ_{adh} (= F_{adh} / W) generated by the meniscus is given by,

$$\mu_{adh} = K_1 \eta V \quad (9)$$

Fig. 28 shows the friction coefficient measured with meniscus force against shear velocity using four liquids proposed by Kawahara [26], where the viscosity of liquids is varied as 56.0 for Propylene glycol, 16.1 for Ethelene glycol, 3.34 for Hexadecane and 0.71 for Nonane using mPa.s units. In Fig. 28, the adhesive friction coefficient given by the meniscus force increases almost proportionally with velocity depending on viscosity, the higher the viscosity, the faster the friction coefficient increases. However, when considering a much longer velocity range, as discussed in greater detail in Fig. 31 and Fig. 32, it takes a considerably longer time for the formation of meniscus for the high viscus uncross-linked phase. Therefore, the velocity dependence of the adhesive friction coefficient might be predicted to be the product of the velocity dependence of the meniscus force itself and the inverse of the time dependence (i.e. the velocity dependence) for the meniscus formation.

Thus, we make an exchange equation (9) with the next equation (10),

$$\mu_{adh} = K_1 \eta V^m \quad (10)$$

When considered the cross-linked rubber, η is the viscosity of the uncross-linked phase and the value m is roughly given depending on the velocity range resulted from Fig.32 given later, m=1 when $V<10^2$ mm/s, m=0 for 10^2 mm/s$\leqq V\leqq 10^4$ mm/s and m=-1 for $V>10^4$ mm/s. The essential difference between Moore's equation (2) and equation (10) originates from the different standpoint for determining the frictional behavior of rubber. That is, the former emphasizes the viscoelastic characteristics of the bulk rubber material such as the modulus and tan δ, which is based on the idealized concept of homogeneous molecular network structure, whilst ignoring the surface conditions. In contrast the latter focuses on the real interfacial characteristics between rubber and solid, specifically to the liquidlike uncross-linked phase on which the meniscus is easily and immediately formed.

4.2.2 Deformation term in the updated rubber friction model

In the classical theory of rubber friction the deformation behavior with hysteresis loss is considered to occur when rubber contacts a hard, solid, rough surface as it slides over the surface's irregularities. In practice, however, the deformation of rubber in frictional sliding occurs more intensely and periodically during stick-slip motion. As shown in Fig. 11 through to Fig. 14 and Fig. 20, the maximum deformation of rubber component results from the resultant vector to the horizontal deflection and vertical indentation during stick-slip motion, where the rubber component of the cyclical extension and retraction is the elastic cross-linked phase in the cross-linked rubber. In this situation, although the adhesive force generated on the cross-linked phase (van der Waals force) is so small that the force cannot sustain a large deformation of a spring (cross-linked phase), however, it might be possible, if the surrounding uncross-linked phases help to adhere the spring to the solid surface more securely, as is shown schematically in Fig. 29.

By considering that the work done to deform such a spring equals to the elastic energy stored in the spring system, then the energy loss *Q* generated in this deformation can be approximated as,

$$Q = \frac{1}{2}\sigma\lambda A h = \frac{1}{2}E\lambda^2 A h \quad (11)$$

where E is the modulus of the cross-linked phase, σ is the maximum stress required to extend an element of area A to a distance λ and *h* is a hysteresis ratio (defined as hysteresis energy dissipated / input energy), which can be equated to tan δ under small cyclic deformations. Thus, when the external work done by shear force F to yield the sliding distance λ is Fλ, the frictional force for deformation F_{def}, together with equation (11), can be approximated as,

$$F_{def} = \frac{1}{2}E\lambda A\tan\delta \quad (12)$$

Moreover, when the maximum deflection produced by stick-slip distance λ equals to $\sqrt{2}d_{s\text{-}s}$ as is the case shown in Fig. 29, then

$$F_{def} = \frac{\tan\delta}{\sqrt{2}} E d_{s\text{-}s} A \quad (13)$$

Now by considering that the stick-slip distance $d_{s\text{-}s}$ is determined by the adhesive characteristic of the surface, the modulus of rubber and normal load as shown in Fig. 13, Fig. 14 and Fig. 20, an additional relationship can be introduced where $d_{s\text{-}s} = k_1 \mu (W/E)^{1/2}$. In addition, if the deformation of the cross-linked phase obeys the Hertzian contact of a sphere, given as $A=k_2E^{-2/3}W^{2/3}$, then the deformation friction coefficient is revealed to be,

$$\mu_{def} = \frac{\tan\delta}{\sqrt{2}} K_2 \mu E^{-7/6} W^{1/6} \quad (14)$$

where k_1, k_2 and K_2 (=k_1k_2) are all coefficients. Equation (14) indicates that the deformation term μ_{def} increases greatly as E decreases and slightly as W increases.

4.2.3 Crack formation term in the updated rubber friction model

As shown in Fig. 8, Fig. 15, Fig. 16, Fig. 18 and Fig. 20, crack formation during stick-slip motion can not be ignored in rubber friction. According to Rivlin & Thomas [27], the elastic energy available to drive a crack, *G* is defined mathematically as

$$G = -\left(\frac{\partial \xi}{\partial S}\right)_l \quad (15)$$

where ξ is the total strain energy stored in a specimen containing a crack of the area S of one fracture surface and the partial derivative indicates that specimen is held at a constant length l. The quantity G known as the strain energy release rate or tearing energy is calculated according to the geometry of specimen. In the strip type specimen that contains a short edge crack of length c under extension, *G* is given,

$$G = 2K_\varepsilon c W_E \quad (16)$$

where K_ε is a constant or a slowly varying number between 2 and 3 and W_E is the strain energy density stored in the specimen without a crack.

When considered that fracture actually occurs on the elastic cross-linked phase in cross-linked rubber shown in Fig. 29, the stored strain energy W_E to extend a fundamental area of the cross-linked phase A to the distance λ is given by $W_E = (1/2) E\lambda^2 A$, and accordingly, *G* can be approximated to,

$$G = K_\varepsilon cE\lambda^2 A \quad (17)$$

Since *G* equals the external work Fλ in rubber friction, the frictional force for crack formation F_{crac} is given as,

$$F_{crac} = K_\varepsilon cE\lambda A \quad (18)$$

Therefore, by adopting the previous approximations used in equation (13), whereby $\lambda = \sqrt{2}d_{s\text{-}s}$, $d_{s\text{-}s}$=

$k_1 \mu (W/E)^{1/2}$, $A=k_2E^{-2/3}W^{2/3}$ and K_2 ($=k_1k_2$), then the crack formation term in the friction coefficient becomes,

$$\mu_{crac} = \sqrt{2}K_\varepsilon K_2 c\, \mu\, E^{-7/6} W^{1/6} \quad (19)$$

Equation (19) also indicates that the crack formation term μ_{crac} increases greatly as E decreases and slightly as W increases.

4.2.4 Comparison of the three components in the rubber friction

The total friction coefficient μ_{all} for the rubber friction is therefore given by the summation of these three components, the adhesive friction coefficient μ_{adh}, the deformation friction coefficient μ_{def} and the crack formation friction coefficient μ_{crac}, according to equation (4) and (5),

$$\mu_{all} = \mu_{adh} + \mu_{def} + \mu_{crac}$$

$$= K_1\eta V^m + K_2 \left[\frac{\tan\delta}{\sqrt{2}} + \sqrt{2}K_\varepsilon c \right] \mu\, E^{-7/6} W^{1/6} \quad (20)$$

A first step is to make a rough estimation of the relative weight of these three terms in a real rubber friction. Although such an estimation is very important and highly desirable, such a trial, however, has never previously been undertaken. Initially, equation (20) is exchanged with equation (21) by assuming $\mu = \mu_{adh}$, because μ_{adh} contributes predominantly to μ ($= \mu_{all}$) at a small normal load, thus accordingly all the three terms in equation (19) can be given as functions of μ_{adh} as,

$$\mu_{all} \fallingdotseq \mu_{adh} \left[1 + K_2 \left(\frac{\tan\delta}{\sqrt{2}} + \sqrt{2}K_\varepsilon c \right) E^{-7/6} W^{1/6} \right] \quad (21)$$

Moreover, several of the parameters in equation (21) are made dimensionless by substituting E, W and c by E/E_0, W/W_0 and c/c_0 respectively. In addition, initial estimates are established for $E/E_0=1$, $W/W_0=1$ and $K_1=1$, $K_2=1$, $K_\varepsilon = 2.5$ to examine similar friction conditions for the three terms. As a result, equation (21) may be written as,

$$\mu_{all} = \mu_{adh} \left[1 + \frac{\tan\delta}{\sqrt{2}} + 2.5\sqrt{2} \left(\frac{c}{c_0} \right) \right] \quad (22)$$

where a potential preexisting defect size in rubber c_0 is assumed to be 50 μm [28] and each crack size c is observed on a rubber surface after a single sliding.

Table 1 gives data necessary to calculate equation (22) for three rubber compounds, NR1 (NR gum), NR2 (NR filled with 20phr of HAF carbon black) and NR3 (NR filled with 50phr HAF carbon black). The table also shows the calculated results for the three terms. The first observation is that the contribution of the deformation term and the crack formation term depends on the physical and mechanical properties of the compound. That is, the deformation term increases with carbon black content due to the increase of tan δ and in contrast the crack formation term decreases with carbon black, because the crack growth rate is suppressed significantly by filling with carbon black. However, in any compounds, the total contribution from the deformation and crack formation is 0.20～0.25

compared with 1.0 for the adhesion term, and hence the weight fraction of the adhesion term to the other two terms is roughly 0.8 to 0.2. Although these calculations include many assumptions and the result is effectively only an initial zeroth order approximation, it might be concluded that the adhesion term is the dominant factor for determining rubber friction, which may typically generate almost 70 ～ 80 % of the total friction coefficient for a cross-linked rubber, except when the normal load is markedly large.

4.3 New interpretations for frictional behaviors of rubber using the new theory

4.3.1 Normal load dependence of friction coefficient

It is now important to create a new interpretation of the frictional behavior of rubber based on this newly derived concept and theory. Initially, the normal load dependence of the friction coefficient is considered. Fig. 30 shows the normal load dependence of friction coefficient for 9 species of rubber and a gelatin proposed by Denny [29], where there is a single master curve which covers 10 materials by normalizing the normal pressure P (=W/area of specimen) by P/E_0, where A is a coefficient and E_0 the compression modulus of material. By assuming that the rubber is an elastic body that behaves as a Hertzian contact of a sphere, μ is seen to be proportional to $W^{-1/3}$. In practice, after Schallamach [30] proposed this relation, it has been widely adopted. However, Fig. 30 shows that the master curve can be divided into three loading regions with different relationships, that is a the logarithmic relation between μ and P is revealed as $\mu = k'_1 W^0$ in the P_1 region, $\mu = k'_2 W^{-1/3}$ in the P_2 region and $\mu = k'_2 W^{-1}$ in the P_3 region, where the three regions are divided by the authors.

When a real interface between a solid and the surface of cross-linked rubber as shown in Fig. 25, Fig. 26 and Fig. 29, the first contact occurs between the solid and the surface of uncross-linked phase to produce a meniscus at a small normal load, where the meniscus area is assumed to increase proportionally with load and hence μ is independent of normal load as is the case in the P_1 region. The second contact of the solid is with a top point of a cross-linked phase of hemisphere (Fig. 26, Fig. 29) at a considerably larger normal load, where μ is proportional to $W^{-1/3}$ in the P_2 region. At a higher normal load, the solid may contact with top surface area of the cross-linked phase of a column shape, where μ is proportional to $W^{-1/2}$ according to the Hertzian contact and finally it comes to be proportional to W^{-1} . This is similar to the situation where a cloud first covers the top of the highest mountain and then as it descends it encounters the lower mountains within the range.

When the normal load increases, the contribution from both the deformation and crack formation terms increase slightly, but the adhesion term decreases more markedly, resulting in the great reduction of the total friction coefficient μ_{all} as shown in Fig. 30, which corresponds to a change of the leading role from the uncrossed-phase to the cross-linked phase as the normal load is increased. Fig. 30 shows that the same normal load dependence is also observed in gelatin, which indicates again that the surface of cross-linked rubber is similar to that of the gelatin, being covered with liquid like materials.

4.3.2 Velocity dependence of friction coefficient

By considering that the adhesion term resulting from meniscus formation plays a dominant role in rubber friction, it might be plausible to accept that the velocity dependence of friction coefficient also results from this meniscus formation. The adhesive frictional force generated by the meniscus increases almost proportionally with increasing velocity as given by equation (9) and Fig. 28 after the meniscus has been completely formed. Conversely, it takes a relatively long time for a highly viscous liquid such as the uncross-linked phase to form the meniscus. Therefore, the velocity dependence of the adhesive friction coefficient might be predicted to be the product of the velocity dependence of the meniscus force itself and the inverse of the time dependence (i.e. the velocity dependence) for the meniscus formation.

Gent and Kim [31] measured adhesive energy G_a dissipated during the impact and rebound of a pendulum to the surface of uncross-linked rubber, known as the tack force for an uncross-linked rubber, calculated using the impact and rebound velocity of a pendulum. In Fig. 31 two kinds of adhesion force are plotted against contact time, one being an auto-adhesion strength between the same uncross-linked rubbers and another an adhesion strength between uncross-linked rubber and metal surface. In this case, the adhesion that is applicable between the uncross-linked phase and solid surface is considered. Initially, the adhesion time in Fig. 31 is divided into six regions by the authors, each with a different slope on the plot of *log* G_a against *log* contact time τ , with each region being given an assigned value for the slope *n* as given in Table 2.

Next an inversion of the horizontal axis between the left and the right in Fig. 31 allows a conversion of the contact time τ into the contact velocity V, whereby the diameter of specimen in the test was assumed to be of the order of 1mm so that 1 sec^{-1} corresponds to 1 mm/sec. The slope *n* on the relation between *log* G_a and *log* τ is therefore converted into *-n* on the relation between *log* G_a and *log* V. In addition, since the meniscus force (corresponding to G_a) is proportional to V^1, the incline of the product of the velocity dependence of the meniscus force and the velocity dependence of the meniscus formation is given by 1-*n*, which is also shown in table 2.

Fig. 32 shows the adhesion friction coefficient μ_{adh} (= μ_m, for meniscus formation) against *log* V over the six regions based on the date from Table 2 represented by thick filled line, where the μ_{adh} value between two velocity regions is approximated by a straight line and the maximum value of μ_{adh} at a peak flat region is determined to be 1.65, corresponding to the saturated maximum value from Sakai's data at 25°C. In the thick filled line, μ_{adh} begins to increase gradually at around 10^{-3} mm/s and comes up to the maximum value at around 10^{2} mm/s, where the maximum flat region continues around 10^{4} mm/s and after the flat region, μ_{adh} decreases again at the velocity of 10^{4}～10^{5} mm/s. This reduction of the friction coefficient at a very high velocity results from the circumstance that at such a very short contact there is insufficient time for the meniscus formation.

Sakai's data (Fig.4) is also plotted in Fig. 32, where it is shown to have a good agreement between the calculated values (thick filled line) and Sakai's data (dashed line) except at the lowest velocity regions of less than 1 mm/s. The reason that Sakai's data is used for this comparison with the calculated results, as mentioned before, is that Sakai's data is only an experimental data available in the literature that shows the velocity dependence of the friction coefficient of the rubber measured directly up to a high velocity region without using a WLF transform. Also on Fig. 32 is plotted another data set estimated from Fig. 24 with the dotted line assuming that μ_{adh} is proportional to the adhesive energy in peeling ($\Delta\gamma$) and the maximum value of μ_{adh} is also to be 1.65, where again there is an excellent agreement between this estimated (dotted line) and the previously calculated (thick filled line). These results indicate that the velocity dependence of friction coefficient of cross-linked rubber can be explained rationally using the present new theory as shown in Fig. 32, whose relation is represented by equation (10). This might suggest undoubtedly that the frictional adhesion force does result from the meniscus force created on the surface of the uncross-linked rubber phase.

One effect that cannot be ignored is that when considering the friction coefficient at the very highest sliding velocities, care must be taken to mitigate the effect of a large temperature rise, which lowers the viscosity of the meniscus, resulting in the marked reduction of the friction coefficient, whose effect may be larger than the reduction of the frictional force caused by insufficient meniscus formation shown in Fig 32. In addition, it is worth noting that the relationship between the negative slope appeared at around $10^4 \sim 10^5$ mm/s in the $\mu \sim$V relation as shown in Fig. 32 and the intense stick-slip motions also appear at a velocity higher than $10^4 \sim 10^5$ mm/s as indicated by Barquins and Roberts. In frictional sliding of rubbers, stick-slip motion occurs under almost all sliding conditions even with a positive slope in the $\mu \sim$V relation, because of the big difference between the static friction coefficient after a long dwell contact time and a dynamic friction coefficient over a much shorter contact time. However, it is well known that the stick-slip motion is greatly amplified under the negative slope conditions and it is quite plausible that a more intense stick-slip motion arises at the velocity region of $10^4 \sim 10^5$ mm/s, as a consequence of the negative slope in Fig. 32.

4.4 Indivisible relationship between friction and wear of rubber

4.4.1 Background of researches of rubber wear

Although rough surfaces of materials such as ceramic, metal, stone, wood and plastic, are made smoother by repeated friction or abrasion with a hard solid, in contrast for rubber materials, when the smooth surface of rubber is abraded, beautiful periodic parallel ridged profile, known as the abrasion pattern, is formed on the rubber surface perpendicular to a sliding direction of the hard solid over the rubber surface as shown in Fig.33. The geometry of the abrasion pattern remains almost constant in appearance after it has grown up to the critical size called a steady state abrasion. The abrasion pattern moves very slowly along in the sliding direction in a manner that the crack at the root of the pattern

wedge is deepened somewhat and the protruding flap is torn off as wear debris as shown in Fig.34, where the growth of two ridges A and B are shown under the increase of the number of contacts. Fig 35 shows the length of the ridge D_{rid} for the ridge A and B observed in Fig. 34 against the number of contacts N. Of course, the difference between the maximum length and the minimum length of ridges in Fig 35 corresponds to the size of the particles of wear debris torn out from rubber, which is about 400 μ m for A and about 1,000 μ m for B, such an increase and decrease of ridges being repeated on the rubber surface in the steady state wear .

Although the close relation between stick-slip motion and abrasion pattern formation was first pointed out by Schallamach［1］through his needle scratch tests, his results were almost ignored by researchers at that time as a special case of rubber wear. In place of it, the major discussion concerning the rubber wear was focused on the fracture mechanic treatments proposed by Thomas et al.［32］, where the rate of wear was related to the crack growth rate of a single ridge using the relation between the strain energy release rate and frictional force. This concept of the crack growth rate greatly contributed to the understand of the rubber wear [33-35]，however this treatment did not consider the initiation and propagation of the abrasion pattern, which left many of the fundamental questions concerning real wear phenomena unresolved. For example, why does the wear of rubber always generate the formation of an abrasion pattern, what is their relationship and what is the driving force required to promote the abrasion pattern. For these technical trends in the research of rubber wear, Fukahori and Yamazaki［36］advocated an indivisible relation among the stick-slip movement, the abrasion pattern formation and the wear of rubber experimentally and theoretically, and later Coveney and Menger［37］ confirmed experimentally the importance of the proposal given by Fukahori and Yamazaki.

4.4.2 Microcracking to abrasion pattern formation in wear of rubber

This paper focuses on the relation between abrasion pattern formation and wear in relation to the characteristics of rubber friction, because it is undoubtedly true that wear is generated by friction. The apparatus used for the wear of the rubber is the same as the previous experiments adopted by Fukahori and Yamazaki［19］as shown in Fig. 36. A rubber block specimen is fixed on a high damping steel plate that moves forward and backward along a horizontal linear path. A steel slider of razor blade type held in a clamp at the end of a rigid cantilever beam is placed on the surface of the movable specimen. The normal load applied by a dead weight that is put directly on the slider. The frictional force is monitored continuously by means of a tangential deflection of spring connected to the slider on which a strain gauge is fixed. When the specimen reaches the end of a horizontal path, the slider is lifted away from specimen whilst the specimen returns to the original position, thus allowing the procedure to be repeated. An acceleration transducer is bonded to the surface of the rubber specimen to monitor the vibration of high frequency. The curvature of the edge of the blade type slider is 0.1 R.

All the experiments were carried out at room temperature (22°C) with a sliding velocity of 20mm/s.

As explained in Fig.8 and Fig.16, the initial microcracks are created on the surface of rubber after just a single pass of the slider. The distance between the periodic microcracks is the same as the period of the high frequency vibration, resulting from the impact of the edge of slider with the top of the vibrating wavy rubber surface as shown schematically in Fig.16. Fukahori and Yamazaki［19] showed how the microcracks thus initiated grow up with the increase of the number of contacts between the rubber and the blade slider as shown in Fig.37. The distance (spacing) between the initial microcracks D_{micro} (35 μ m) increases up to the final (steady) abrasion pattern spacing D_{ab} (2600 μ m) at around 1500 cycles. After reaching the steady state condition it is approximately constant, where the initial spacing and the final spacing agree well with the period (distance) of the high frequency vibration d_{h-v} and the stick-slip motion (stick-slip distance) d_{s-s}, respectively. Conversely, Fig. 38 shows the rate of wear loss (volume/cycle) $\dot{V}$ plotted against the number of contacts N, which has the same tendency as observed in Fig.37. The rate of wear increases gradually from an initial small value to the steady one at around 1500 cycles, after then it is also approximately constant. The similar results observed in Fig.37 and Fig.38 suggest that the growth of wear is closely related to the propagation of the abrasion pattern. In other words, the wear depends essentially on the growth of the abrasion pattern, and in addition the size of abrasion pattern is decided by the stick-slip distance generated by stick-slip motion. As a conclusion it can be stated that the rubber wear is also governed by the stick-slip motion.

Additional experiments were carried out to confirm whether the above relations were always established generally. Fig.39 shows the relation between the distance between the initial microcracks (D_{micro}) and the period (distance) of the high frequency vibration (d_{h-v}) for six rubber compounds at 30N, indicating that both values are almost completely in agreement. In addition, Fig.40 shows the relationship between the abrasion pattern distance at a final steady state (D_{ab}) and the stick-slip distance (d_{s-s}) for six rubber compounds and four normal loads condition, indicating that both the values are in also almost complete agreement. Thus, it is proposed that there is an universal process for all rubber compounds under normal loading conditions that the abrasion pattern is initiated as microcracks by a small amount of energy supplied by the high frequency vibration, which increases to the stick-slip distance promoted by the much larger energy created by the stick-slip motion. This is then maintained as a steady state abrasion afterwards.

4.4.3 Mechanism of rubber wear correlated with abrasion pattern formation

The relation between the rate of wear ($\dot{V}$) and the abrasion pattern distance (D_{ab}) at a steady state of abrasion and wear was first pointed out by Schallamach［1］, where he proposed an empirical relation,

$$\dot{V}=a\, D_{ab}^{n} \qquad (23)$$

where n=3. After Schallamach, Ratner, et. al.［38］ investigated in more detail and commented that the value of n was changeable according to materials and the contact conditions. Thus, we also

measured the relationship between both parameters for six rubber compounds at 30N and at four normal loads condition at the steady state abrasion. Fig.41 shows the plots of $\dot{V}$ against D_{ab}, where the relationship, $\dot{V}=b\ D_{ab}^{3.5}$ is also shown. In addition, Fig.42 is another measurement using a Lambourn abrasion testing machine under several loads and slip ratios, where the relationship is given as $\dot{V}=c\ D_{ab}^{3.3}$. Although the value of n changes slightly depending on materials and the experimental conditions, it may be reasonable to estimate that n =3.

Now we would like to consider the relation $\dot{V}=b\ D_{ab}^{3}$ theoretically. Fig.43 shows a root of an abrasion pattern at the steady state, where a tip of crack (wedge) progresses to the inside of rubber body with a small angle. Fig.44 simulates Fig.43 schematically, where the tip of wedge consisting of the geometry of the depth $\triangle Y$, the width $\triangle X$ and the length $\triangle Z$ is cut between two ridges perpendicularly to the sliding direction of a blade slider. Since the abrasion pattern spacing equals to the stick-slip distance at the steady state, one stick-slip motion works to open the tip of the wedge as an external driving force. This is similar to the situation that the propagation of tear fracture in fatigue is generated by each repeated extension. Thus it is reasonable to propose that the components of a crack, $\triangle X$, $\triangle Y$ and $\triangle Z$ are all proportional to the magnitude of stick-slip distance (thus equals to the abrasion pattern distance D_{ab}). Since the rate of abrasion (wear) $\dot{V}$ is proportional to the volume of the crack $\triangle V$ ($=\triangle X\triangle Y\triangle Z$), accordingly $\dot{V}$ is proportional to a cube of D_{ab} as given by a power law,

$$\dot{V} = bD_{ab}^{3} \qquad (24)$$

All measurements and theory described in this paper undoubtedly indicate that the rubber wear is generated through the formation of abrasion pattern induced by the stick-slip motion, and thus all the phenomena concerning the friction and wear of rubber are fundamentally originated by the sticky surface of rubber.

5. Conclusion

(1) Different distinctive behaviors in rubber friction such as the much higher fiction coefficient than a plastic and intense stick-slip motion in sliding are all caused by the sticky characteristic of the surface of cross-linked rubber, generated by the formation of a meniscus of the uncross-linked phase in a cross-linked rubber,

(2) Total friction coefficient of rubber μ_{all} consists of three components including an adhesion term μ_{adh}, a deformation term μ_{def} and a crack formation term μ_{crac}, thus given as

$$\mu_{all} = \mu_{adh} + \mu_{def} + \mu_{crac} \fallingdotseq K_1 \eta V \left[1 + K_2\left(\frac{\tan\delta}{\sqrt{2}} + \sqrt{2}K_{\varepsilon} c\right) E^{-7/6} W^{1/6}\right]$$

where η is the viscosity of the uncross-linked phase, E the modulus of the cross-linked phase, c crack length, W normal load, K_1, K_2, K_{ε} are all coefficients and m=1 when $V<10^2$ mm/s, m=0 for 10^2 mm/s$\leqq V\leqq 10^4$ mm/s, m=-1 for $V>10^4$ mm/s.

(3) Under the general conditions, the most significant factor in the above equation is the adhesion term that seems to occupy roughly 70～80 % of μ_{all} according to a very rough estimation, which indicates that the meniscus force brought about at the interface between the uncross-linked phase and solid dominates the sliding system and its frictional behavior of rubbers.

(4) The friction coefficient decreases greatly corresponding to a change of the leading role from the uncross-linked phase to the cross-linked phase as the normal load is increased, resulting in the marked reduction of the total friction coefficient.

(5) The velocity dependence of the friction coefficient can also be determined by the meniscus force, as it can be represented by the product of the velocity dependence of the meniscus force and the inverse of the time dependence (i.e. the velocity dependence) for the formation of the meniscus. An initial rough estimation based on the above assumption shows that μ_{adh} begins to increase gradually at around 10^{-3} mm/s and comes up to the maximum value at 10^{2} mm/s with the increase of velocity, where the maximum flat region continues to around 10^{4} mm/s and after the flat region μ_{adh} decreases again at the velocity of 10^{4}～10^{5} mm/s, whose estimation gives a good agreement with other experimental data.

(6) The similarity between the gel and the cross-linked rubber in the structure and the frictional behaviors strongly suggests that the surface of the cross-linked rubber is also covered with liquid-like material to make a meniscus.

(7) The close relationship between the wear rate, the abrasion pattern formation and the stick-slip motion has been clearly demonstrated by experiments and theory. The abrasion pattern is initiated by the high frequency vibration and the steady abrasion pattern together with steady wear rate is promoted by the intense stick-slip motion.

(8) Wear rate $\dot{V}$ could be estimated theoretically as a function of the abrasion pattern spacing D_{ab} at a steady state wear using a simple equation $\dot{V} = bD_{ab}^{3}$, thus it is concluded that many characteristics of rubber wear are also fundamentally governed by the stick-slip motion induced by the sticky rubber surface. These phenomena have an indivisible relation each other.

References

1. A. Schallamach, Friction and abrasion of rubber, Wear, 1 (1957/58) 384-417

2. K.A. Grosch, The relation between the friction and viscoelastic properties of rubber, Proc. Roy. Soc., A274 (1963) 21-39

3. K.C. Ludema, D. Tabor, The friction and viscoelastic properties of polymeric solids, Wear, 9 (1966) 329-348

4. D.F. Moore, The friction and lubrication of elastomers, Pergamon Press, Oxford, 1972

5. M.L. Williams, R.F. Landel, J.D. Ferry, The temperature dependence of relaxation mechanism in amorphous polymers and other glass-forming liquids, J. American Chem. Soc., 77 (1955) 3701-3707

6. G.M. Bartenev, A.I. Elkin, Friction properties of high elastic materials, Wear, 8 (1965) 8-21
7. M. Barquins, A.D. Roberts, Rubber friction variation with rate and temperature: some new observations, J. Phys, D: Appl. Phys, 19 (1986) 547-563
8. T.V. Tolpekina, B.N. Persson; Adhesion and Friction for Three Tire Tread Compounds, Lubricants, *7*, 20, 2019
9. H. Sakai, Engineering of Tire, Granpri press, 1986, p57
10. K.L. Johnson, K. Kendal, A.D. Roberts, Surface energy and the contact of elastomeric solid, Proc. Roy. Soc. London A 324 (1971) 301-313
11. D. Maugis, Adhesion of spheres: the JKR-DMT transition using a Dugdale model, J. Colloid Inter. Sci., 150 (1992) 243-269
12. D.S. Dugdale, J. Mech. Phys. Solids, 8 (1960) 100-
13. M. Saeki, Research Report of Hyogo-Kenritsu Technical Center, ***23***, 16, 2014
14. Y. Fukahori, Carbon black reinforcement of rubber, (No8) the origin of weakness and reinforcement of elastomers, Nippon Gomu Kyokaishi, 78 (2005) 19-25
15. Y. Fukahori, P. Gabriel, J.J.C. Busfield, How does rubber truly slide between Schallamach waves and stick-slip motion? Wear, 269 (2010) 854-866
16. H. Watabe, M. Komura, K. Nakajima, T. Nishi, Atomic force microscopy of mechanical property of Natural rubber, Japanese J. Appl. Phys., 44 (2005) 5393-5396
17. A. Schallamach, How does rubber slides? Wear, 17 (1971) 301-312
18. M. Barquins, R. Courtel, Rubber friction and the rheology of viscoelastic contact, Wear, 32 (1975) 133-150
19. Y. Fukahori, H. Yamazaki, Mechanism of rubber abrasion. Part1: Abrasion pattern formation in natural rubber vulcanizate, Wear, 171 (1994) 195-201
20. Y. Fukahori, H. Yamazaki, Mechanism of rubber abrasion. Part2: General rule in abrasion pattern formation in rubber-like materials, Wear, 178 (1994) 109-116
21. H. Liang, Y. Fukahori, A.G. Thomas, J.J.C. Busfield, Rubber abrasion at steady state, Wear, 266 (2009) 288-296
22. K.V. Shooter, D. Tabor, The frictional properties of plastics, Proc. Roy. Soc., 65(1952)661-671
23. A.D. Roberts, A.G. Thomas, The adhesion and friction of smooth rubber surface, Wear, 33 (1975) 45-64
24. A. Suzuki, Y. Yamazaki, Y. Kobiki, Direct observation of polymer gel surfaces by atomic force microscopy, J. Chem. Phys., 104 (1996) 1751-1757
25. F.P. Bowden, D. Tabor, The friction and lubrication of solids, Oxford Univ. Pres., 1950
25. S. Kawahara, Improvement of tribological character in lubrication with brush frame, PhD thesis, University of Nagoya, 2014
27. R.S. Rivlin, A.G. Thomas, Rupture of rubber. 1 . Characteristic energy for tearing, J. Polm. Sci.,

10 (1953) 291-318
28. Y. Fukahori, Prediction of fatigue life of elastomer, Nippon Gomu Kyokaishi, 58 (1985) 625-633
29. D.F. Denny, The influence of load and surface roughness on the friction of rubber-like materials, Proc. Phys. Soc. B, 66 (1953) 721-727
30. A. Schallamach, The load dependence of rubber friction, Proc. Phys. Soc. B, 65 (1952) 657-661
31. A.N. Gent, H.J. Kim, Effect of contact time on tack, Rubber Chem. Technol., 63 (1990) 613-623
32. D.H. Champ, E. Southern, A.G. Thomas; Advances in polymer friction and wear, Ed. by L. H. LEE, Plenum, New York and London 1974, p133
33. A.N. Gent, C.T.R. Pulford, Mechanism of rubber abrasion, J. Appl. Polym. Sci., ***28*** (1983) 943-960
34. S.W. Zhang, Rubber Chem. Technol., ***57***, 755, 1984
35. A.H. Muhr, T.J. Pond, A.G. Thomas, J. Chem. Phys., ***84***, 331, 1987
36. Y. Fukahori, H. Yamazaki, Mechanism of rubber abrasion. Part3: How is friction linked to fracture in rubber abrasion? Wear, ***188*** (1995) 19-26
37. V. Coveney, C. Menger, Initiation and development of wear of an elastomeric surface by a blade, Wear, ***233***, 1999, 702-711
38. S.B. Ratner, V.E. Gul, G.S. Klitenick, The abrasion of vulcanized rubber against wire gauze, Rubber Chem. Technol., ***32***, 471, 1959

Captions

Fig.1: Master curve of the coefficient of friction as a function of sliding velocity for Acrylonitrile-butadiene rubber at 20℃, reprinted from ref. [2]

Fig.2: The velocity dependence of coefficient of friction for isomerized NR using a WLF transformation together with Grosch data (dashed line), reprinted from ref. [7]

Fig.3; Friction coefficient as a function of sliding velocity measured at 20℃ for the dry contact and in the water on a smooth glass surface for three rubber compounds, reprinted from ref. [8]

Fig.4: Coefficient of friction as a function of sliding velocity at constant temperature, reprinted from ref. [9]

Fig.5: Contact diameter against normal load between a rubber sphere and a flat rubber surface at around zero applied load, reprinted from ref. [10]

Fig.6; the relation between friction coefficient and stickiness index measured by finger-tip test, reprinted from ref. [13]

Fig.7: Spectra of stick-slip motion (frictional force, upper) and vibration of high frequency (acceleration, lower) against time as a blade slider slides on the surface of a NR vulcanizate, reprinted

the viscosity of liquids being 56.0 for Propylene glycol, 16.1 for Ethelene glycol, 3.34 for Hexadecane and 0.71 for Nonane using mPa・S units, reprinted from ref. [26]

Fig.29: Schematic representation of an elastic unit of the crosslinked phase supported securely by the surrounding adhesive meniscuses of the uncross-linked phase

Fig.30: Relation between a normalized coefficient of friction μA and a normalized normal pressure P/E_0 for 9 species of cross-linked rubber and a gel, A is a coefficient and E_0 a compression modulus, reprinted from ref. [29]

Fig.31: Adhesive energy G_a against contact time τ for the uncross-linked SBR measured at 25℃ using pendulum testing, one being an auto-adhesion strength between uncross-linked rubbers and another an adhesion strength between uncross-linked rubber and metal surface, reprinted from ref. [31]

Fig.32: Coefficient of friction against sliding velocity at 25℃ for the calculation based on Table 2 (thick solid line), together with Sakai's data (Fig.4) (dashed line) and an estimation derived using Fig.24 (dotted line)

Fig.33: SEM photograph of abrasion pattern of NR at a steady state wear, arrow indicating a sliding direction of slider

Fig.34: Sectioned profiles of two ridges (abrasion patterns) of NR propagated with increasing the number of contacts (cycles)

Fig.35: Relation between the length of the ridge D_{rid} and the number of contacts N for the ridge A and B observed in Fig. 34

Fig.36: A hand-made apparatus for measurement of friction and wear of rubber, reprinted from ref. [36]

Fig.37: Abrasion pattern spacing as a function the number of contacts (cycles) for NR, reprinted from ref. [36]

Fig.38: Rate of wear loss (volume/cycle) $\dot{V}$ plotted against the number of contacts N, reprinted from ref. [36]

Fig.39: Relation between the spacing of initial microcracks (D_{micro}) and the period of the high frequency vibration ($d_{h\text{-}v}$) for six rubber compounds

Fig.40: Relation between abrasion pattern spacing (D_{ab}) and stick-slip distance ($d_{s\text{-}s}$) at a steady wear for six rubber compounds at 30 N (white) and for NR (black) at 10N(a).30N(b), 50N(c), 80N(d)

Fig.41: Relation between the rate of wear ($\dot{V}$) and the abrasion pattern distance (D_{ab}) at a steady wear for six rubber compounds at 30N (white) and for NR (black) at 10N(a), 30N(b), 50N(c), 80N(d)

Fig.42: plots of $\dot{V}$ against D_{ab} measured using Lambourn abrasion testing machine,

Fig.43: SEM photograph of a root of an abrasion pattern of BR at the steady wear

Fig.44: Schematic illustration to show a tip of wedge consisting of the depth ⊿Y, the width ⊿X and the length ⊿Z

Table 1: Data for calculation of equation (21) and the calculated results for three rubber compounds,

NR1 (NR gum), NR2 (NR filled with 20phr of HAF carbon black) and NR3 (NR filled with 50phr HAF carbon black)

Table 2: The slope value *n* for the slopes of six period regions divided on the relation between *log* G_a and *log* time in Fig. 33 and 1-*n* for the relation between *log* G_a and *log* V obtained by the product of the velocity dependence of meniscus force and the velocity dependence of the meniscus formation

Figures and Tables

Fig.1

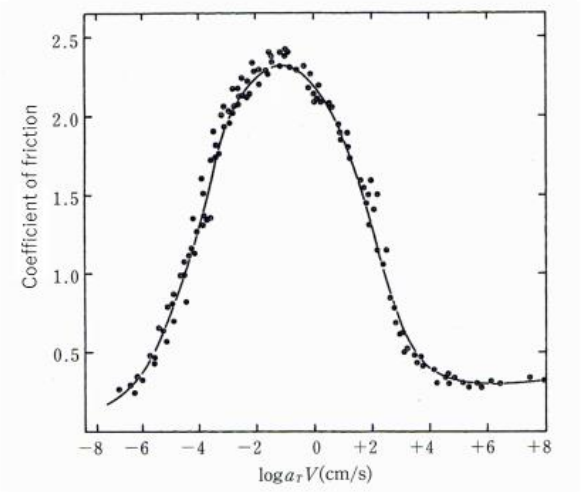

Fig.2

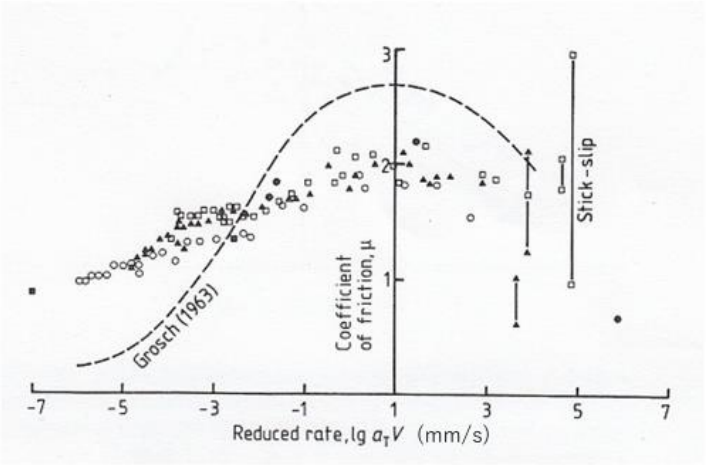

Fig.3

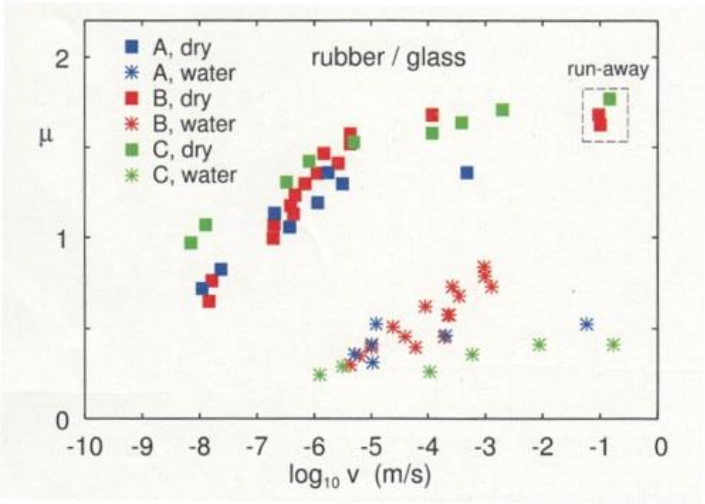
A, dry
A, water
B, dry
B, water
C, dry
C, water
rubber / glass
run-away
μ
2
1
0
-10 -9 -8 -7 -6 -5 -4 -3 -2 -1 0
log10 v (m/s)

Fig.4

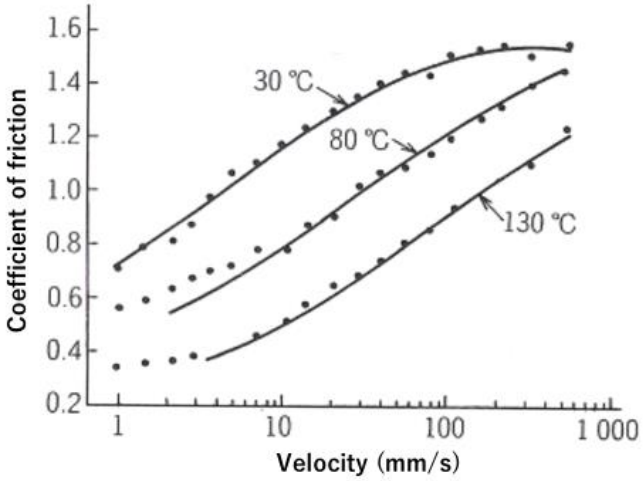
Coefficient of friction
1.6
1.4
1.2
1.0
0.8
0.6
0.4
0.2
30 ℃
80 ℃
130 ℃
1
10
100
1 000
Velocity (mm/s)

Fig.5

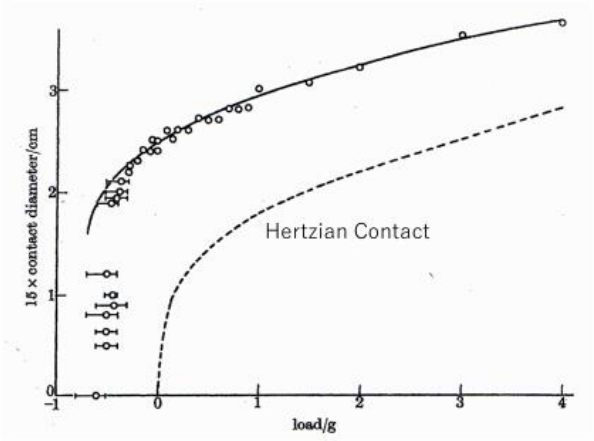
15 × contact diameter/cm
load/g
Hertzian Contact

Fig.6

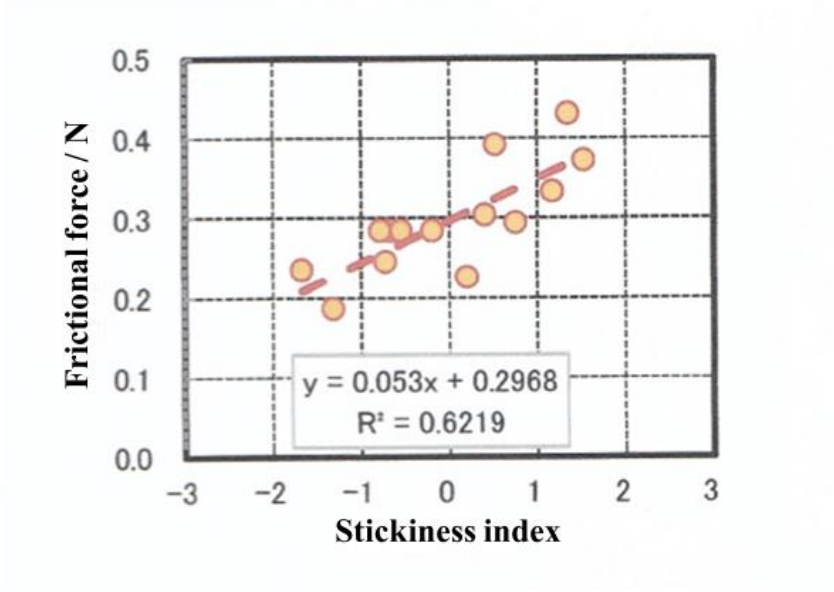
Frictional force / N
Stickiness index
y = 0.053x + 0.2968
R² = 0.6219

Fig.7

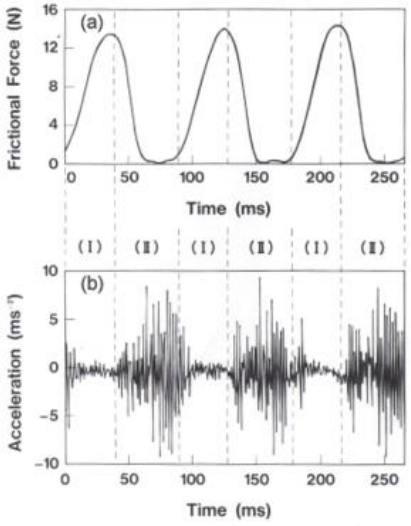
(a)
Frictional Force (N)
16
12
8
4
0
0
50
100
150
200
250
Time (ms)
(Ⅰ)
(Ⅱ)
(Ⅰ)
(Ⅱ)
(Ⅰ)
(Ⅱ)
(b)
Acceleration (ms⁻²)
10
5
0
−5
−10
0
50
100
150
200
250
Time (ms)

Fig.8


20 μm

Fig.9

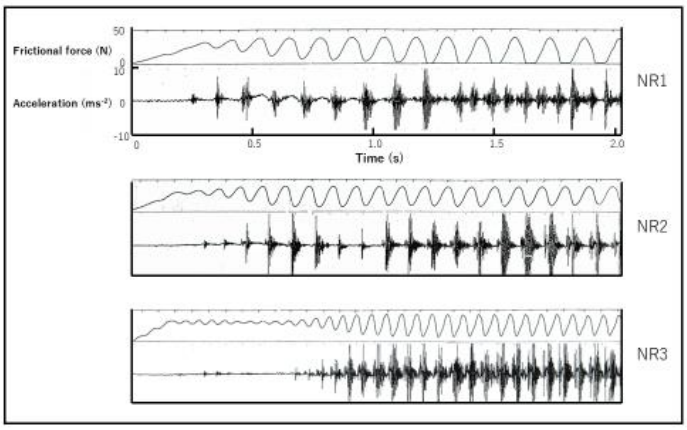
Frictional force (N)
50
0
Acceleration (ms-2)
10
0
-10
0
0.5
1.0
1.5
2.0
Time (s)
NR1
NR2
NR3

Fig.10

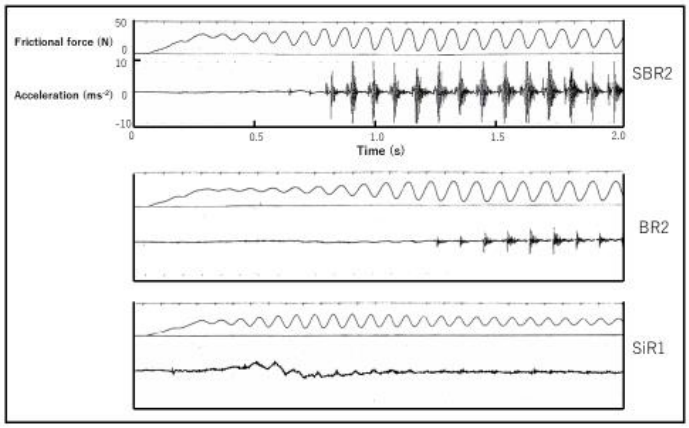
Frictional force (N)
50
0
Acceleration (ms-2)
10
0
-10
0
0.5
1.0
1.5
2.0
Time (s)
SBR2
BR2
SiR1

Fig.11

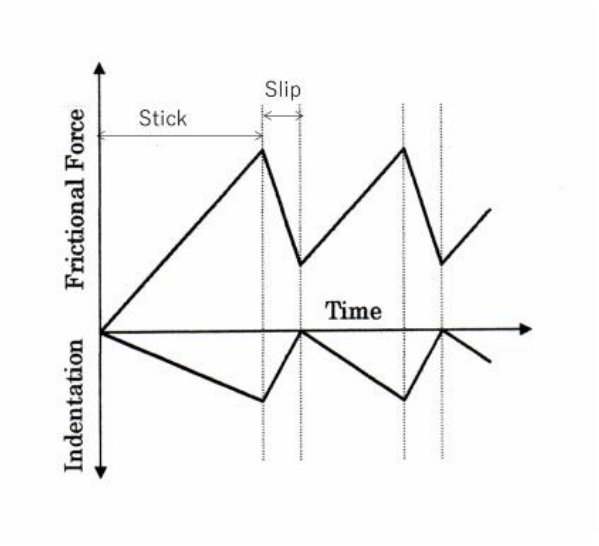
Slip
Stick
Frictional Force
Time
Indentation

Fig.12

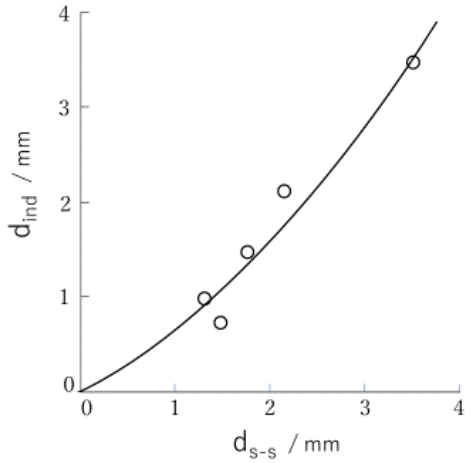
4
3
2
1
0
0
1
2
3
4
d_{ind} / mm
$d_{s\text{-}s}$ / mm

Fig.13

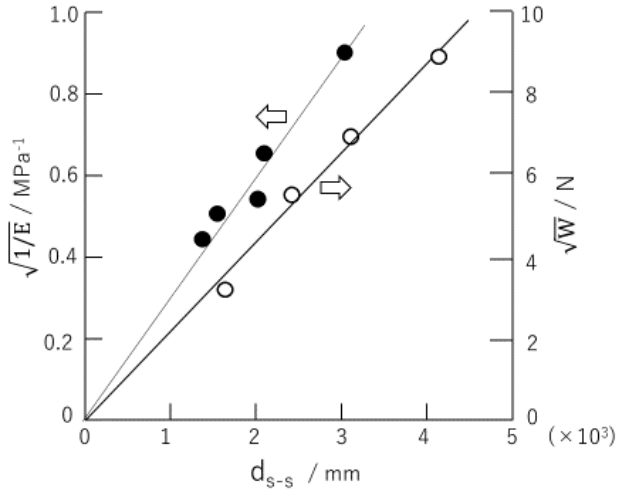
1.0
0.8
0.6
0.4
0.2
0
$\sqrt{1/E}$ / MPa^{-1}
10
8
6
4
2
0
$\sqrt{W}$ / N
0
1
2
3
4
5
(×10^3)
$d_{s\text{-}s}$ / mm

Fig.14

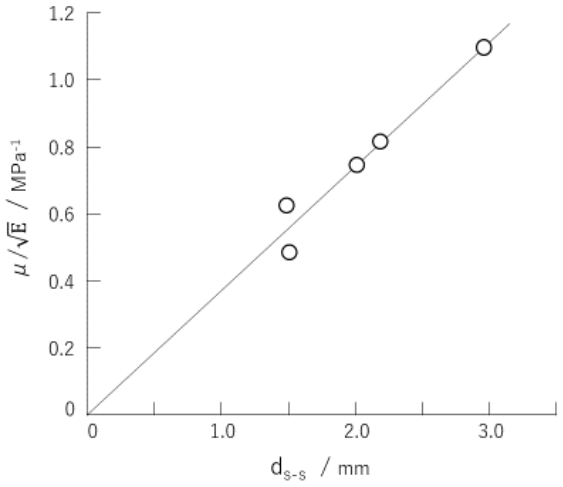
1.2
1.0
0.8
0.6
0.4
0.2
0
$\mu/\sqrt{E}$ / MPa^{-1}
0
1.0
2.0
3.0
$d_{s\text{-}s}$ / mm

Fig.15

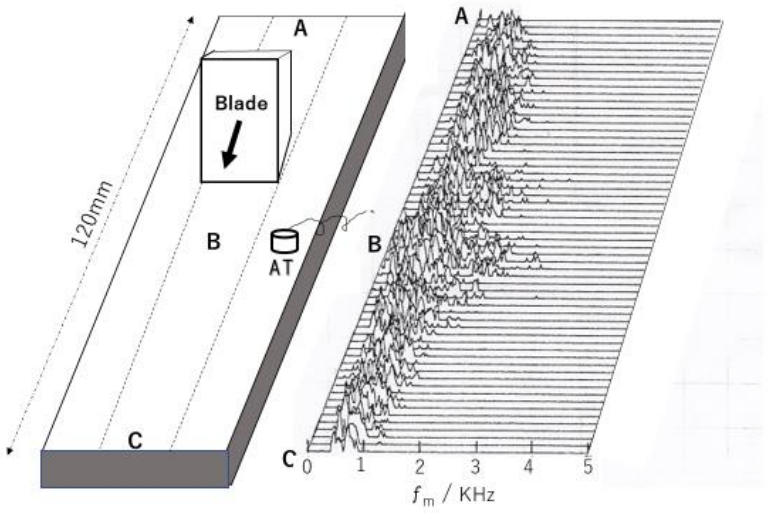
A
Blade
120mm
B
AT
C
A
B
C
0
1
2
3
4
5
f_m / KHz

Fig.16

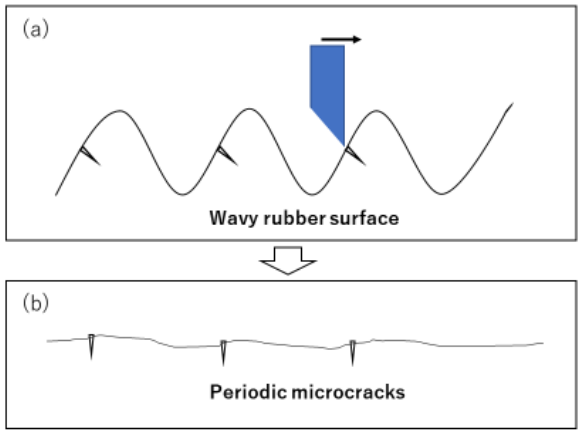
(a)
Wavy rubber surface
(b)
Periodic microcracks

Fig.17

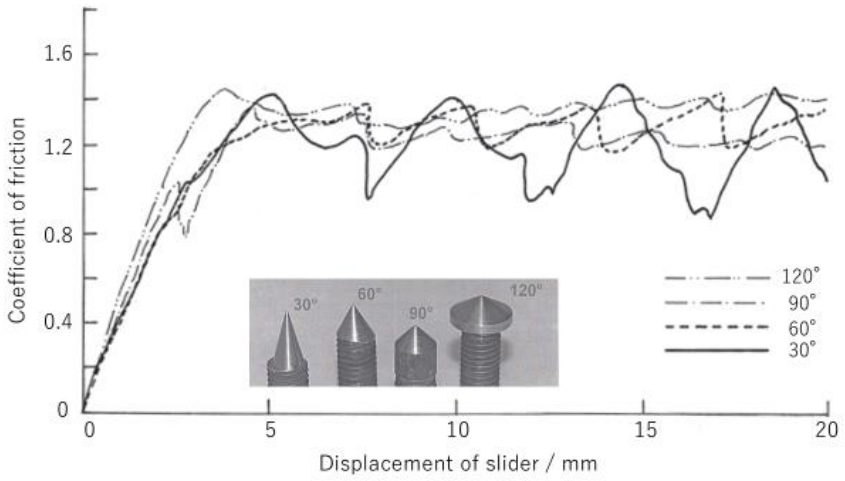
Coefficient of friction
1.6
1.2
0.8
0.4
0
0
5
10
15
20
Displacement of slider / mm
30°
60°
90°
120°
120°
90°
60°
30°

Fig.18

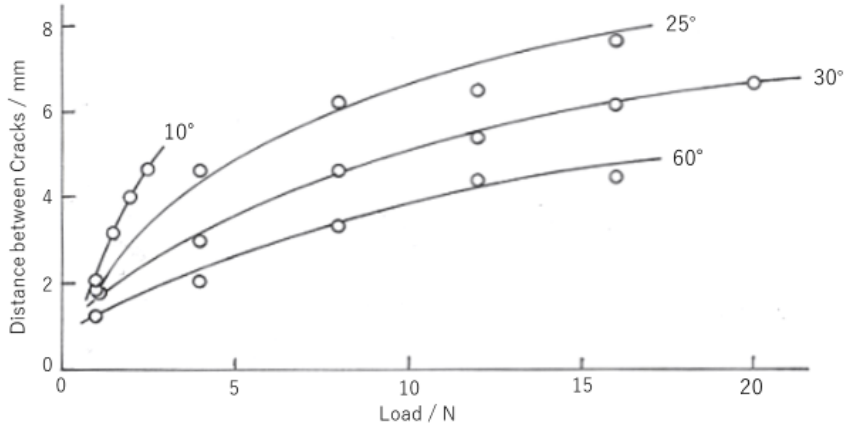
Distance between Cracks / mm
8
6
4
2
0
0
5
10
15
20
Load / N
10°
25°
30°
60°

Fig.19

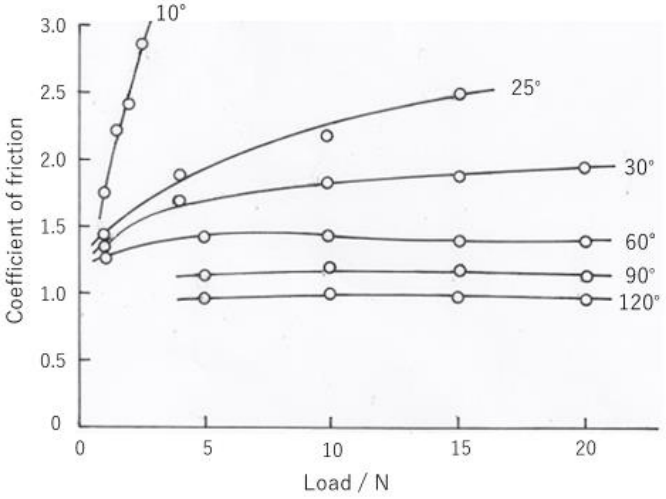
10°
25°
30°
60°
90°
120°
Coefficient of friction
Load / N
3.0
2.5
2.0
1.5
1.0
0.5
0
0
5
10
15
20

Fig.20

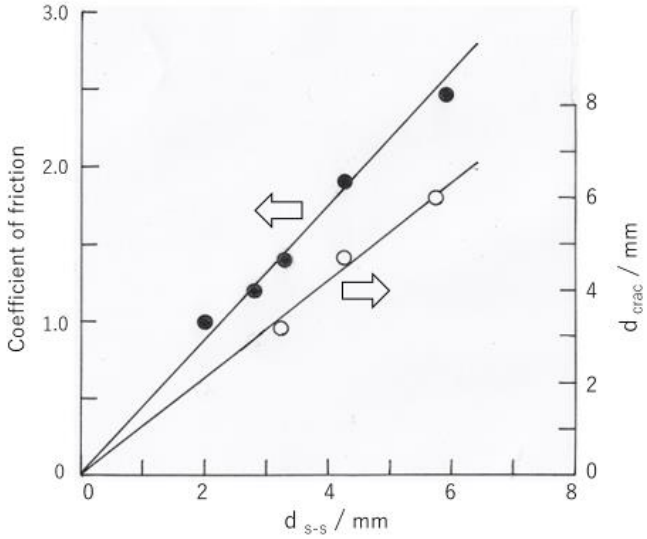
Coefficient of friction
d s-s / mm
d crac / mm
3.0
2.0
1.0
0
0
2
4
6
8
8
6
4
2
0

Fig.21

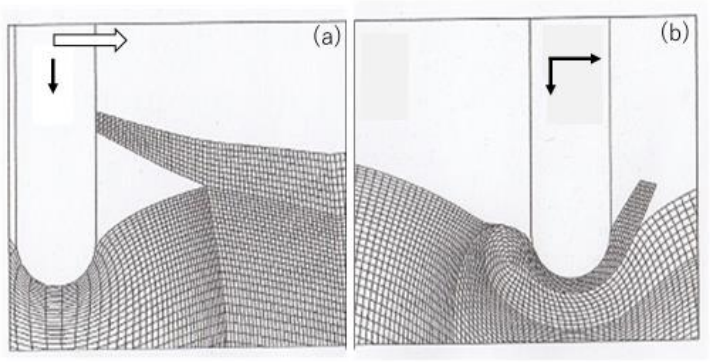
(a)
(b)

Fig.22

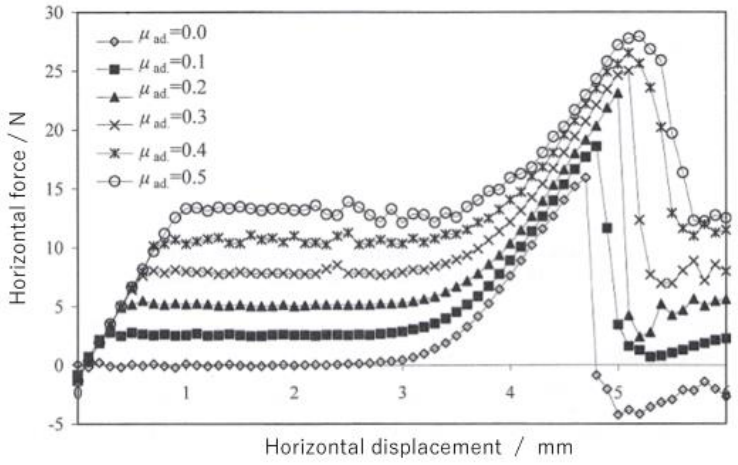
μad.=0.0
μad.=0.1
μad.=0.2
μad.=0.3
μad.=0.4
μad.=0.5
Horizontal force / N
Horizontal displacement / mm
30
25
20
15
10
5
0
-5
1
2
3
4
5

Fig.23

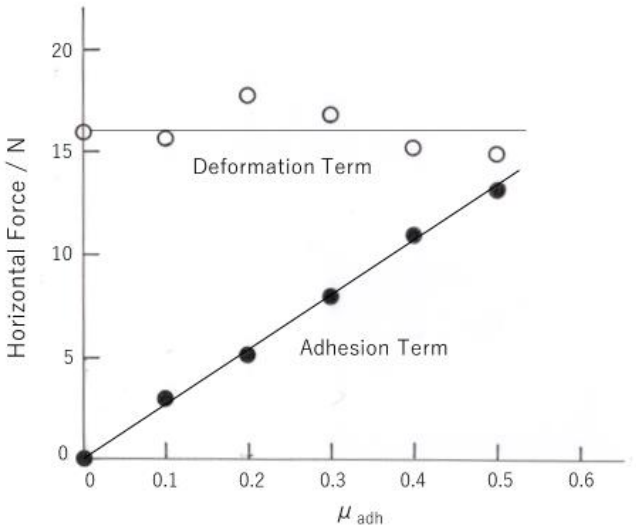
Horizontal Force / N
20
15
10
5
0
Deformation Term
Adhesion Term
0
0.1
0.2
0.3
0.4
0.5
0.6
μ_{adh}

Fig.24

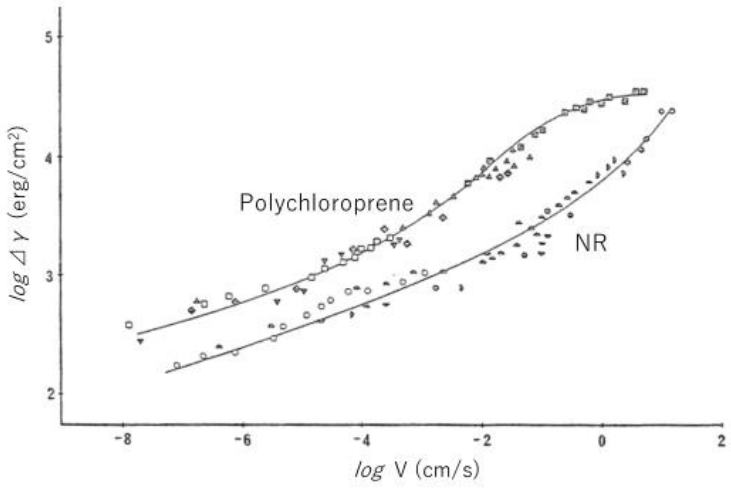
log Δ γ (erg/cm²)
5
4
3
2
Polychloroprene
NR
-8
-6
-4
-2
0
2
log V (cm/s)

Fig.25

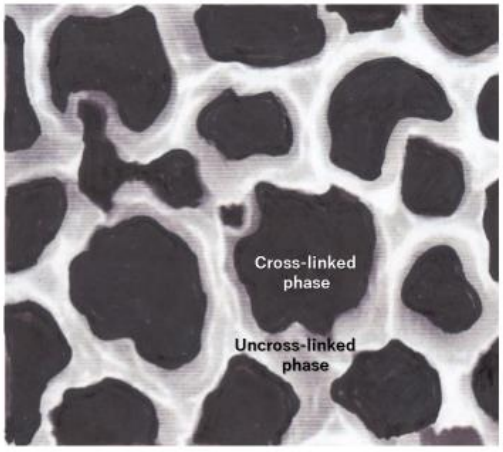
Cross-linked
phase
Uncross-linked
phase

Fig.26

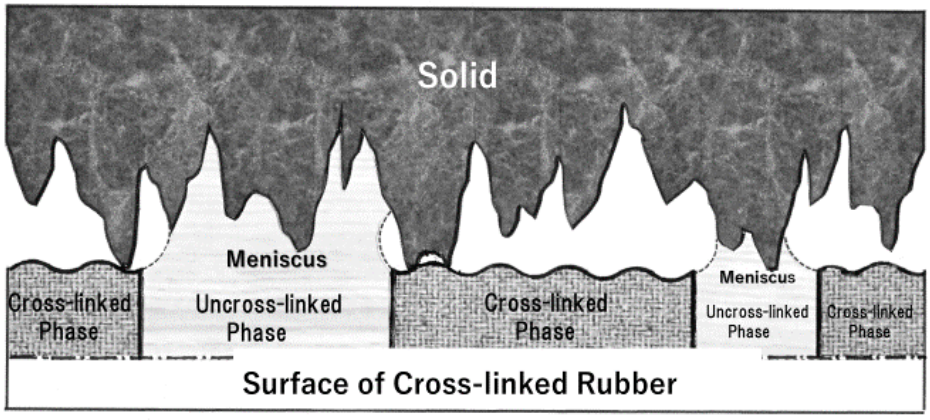
Solid
Meniscus
Cross-linked
Phase
Uncross-linked
Phase
Cross-linked
Phase
Meniscus
Uncross-linked
Phase
Cross-linked
Phase
Surface of Cross-linked Rubber

Fig.27

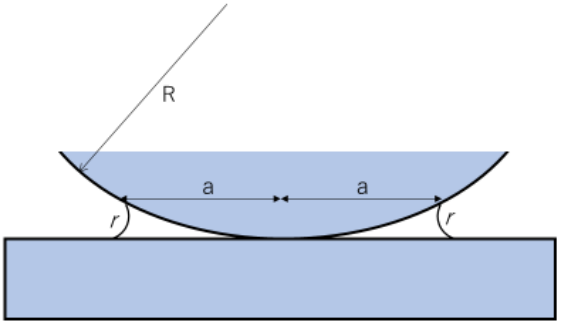
R
a
a
r
r

Fig.28

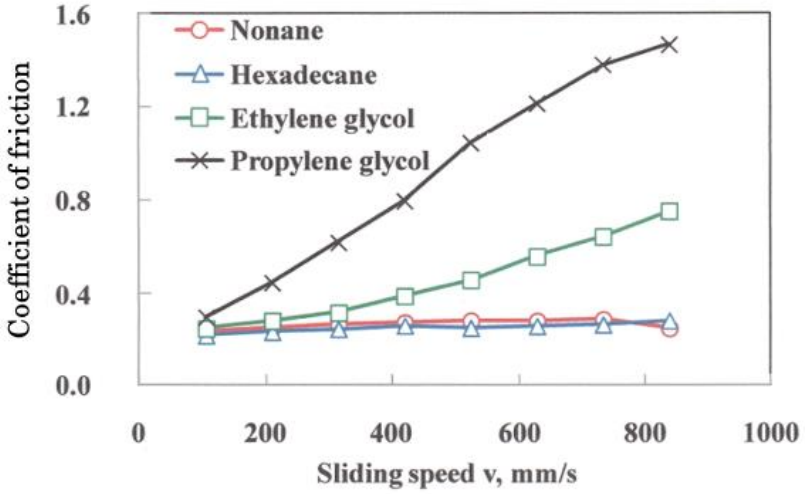
Coefficient of friction
1.6
1.2
0.8
0.4
0.0
Nonane
Hexadecane
Ethylene glycol
Propylene glycol
0
200
400
600
800
1000
Sliding speed v, mm/s

Fig.29

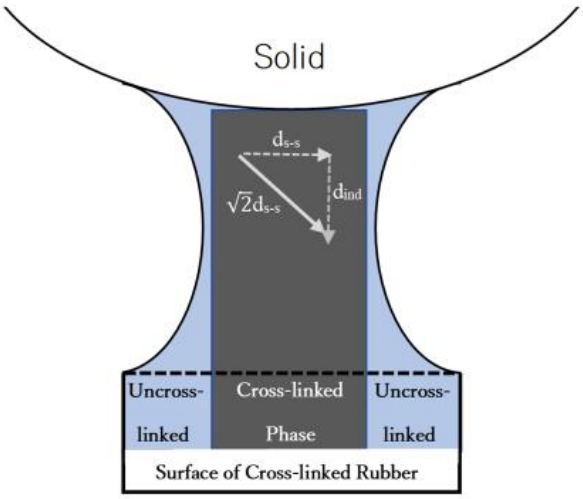
Solid
$d_{s\text{-}s}$
$\sqrt{2}d_{s\text{-}s}$
d_{ind}
Uncross-linked
Cross-linked Phase
Uncross-linked
Surface of Cross-linked Rubber

Fig.30

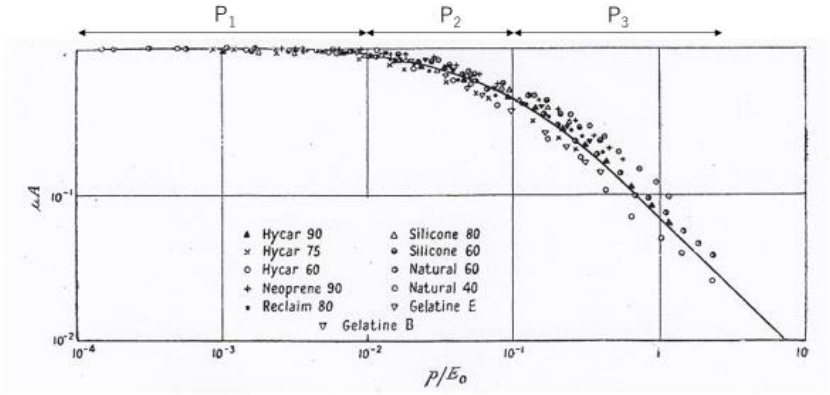
P1
P2
P3
μA
10⁻¹
10⁻²
10⁻⁴
10⁻³
10⁻²
10⁻¹
1
10
p/E₀
Hycar 90
Hycar 75
Hycar 60
Neoprene 90
Reclaim 80
Silicone 80
Silicone 60
Natural 60
Natural 40
Gelatine E
Gelatine B

Fig.31

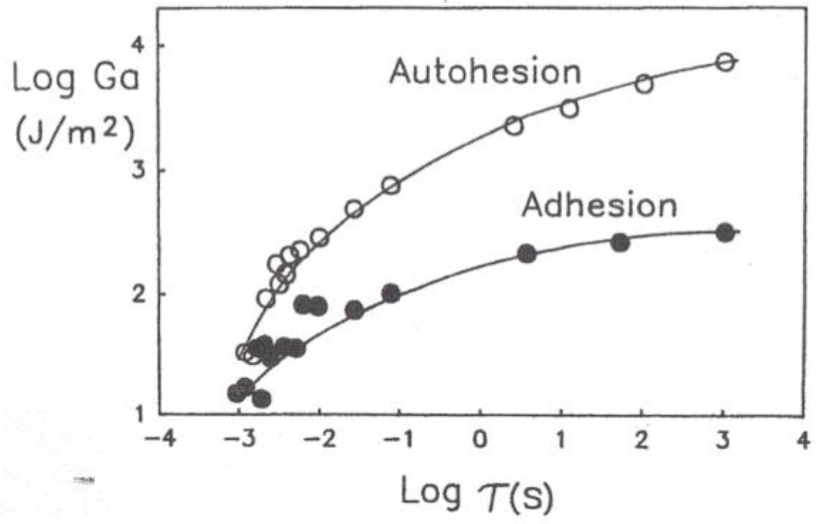
Log Ga
(J/m2)
Autohesion
Adhesion
Log T(s)
4
3
2
1
−4
−3
−2
−1
0
1
2
3
4

Fig.32

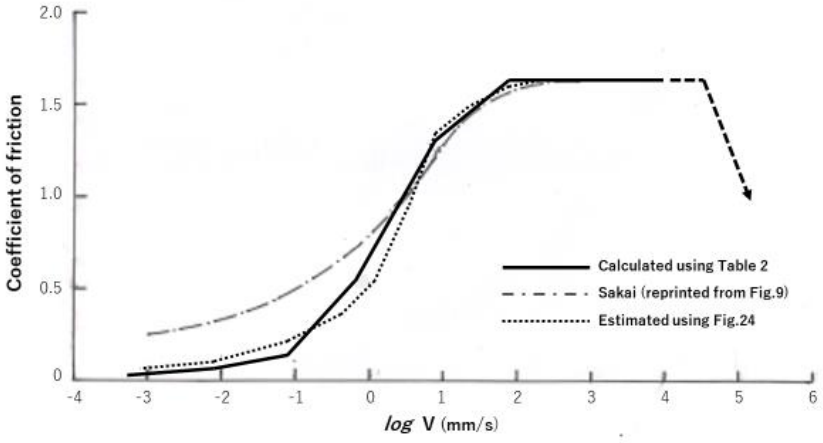
Coefficient of friction
2.0
1.5
1.0
0.5
0
-4
-3
-2
-1
0
1
2
3
4
5
6
log V (mm/s)
Calculated using Table 2
Sakai (reprinted from Fig.9)
Estimated using Fig.24

Fig.33

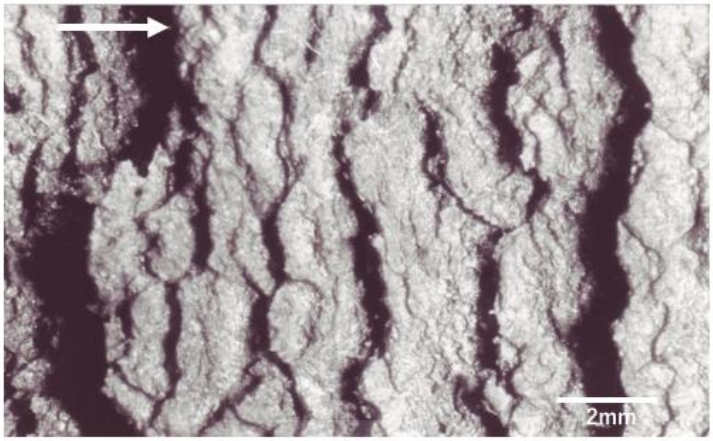

Fig.34

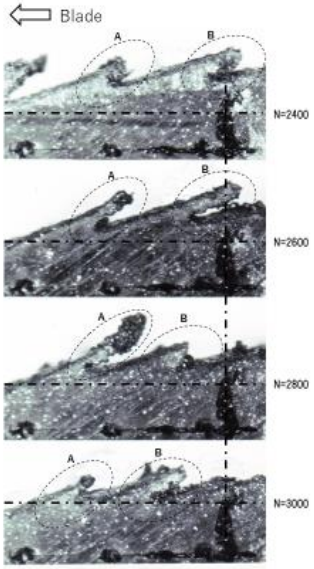

Fig.35

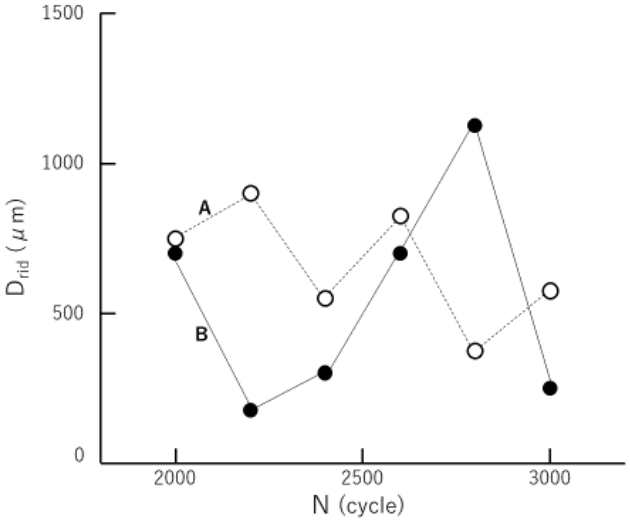
1500
1000
500
0
D_{fid} (μm)
A
B
2000
2500
3000
N (cycle)

Fig.36

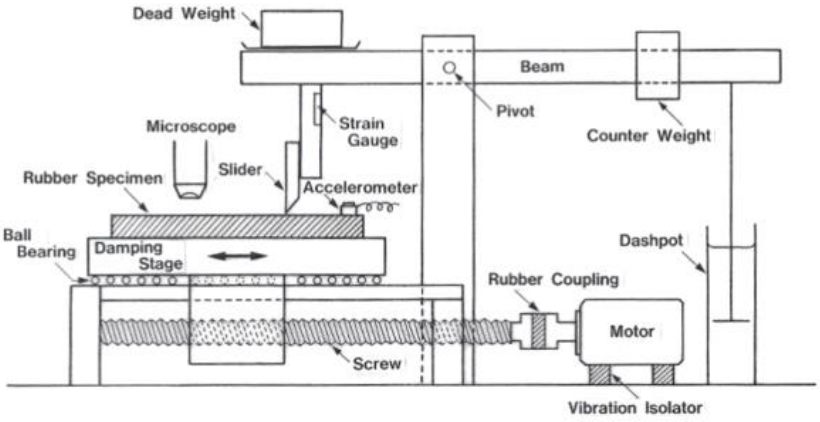
Dead Weight
Beam
Pivot
Counter Weight
Microscope
Strain Gauge
Slider
Rubber Specimen
Accelerometer
Ball Bearing
Damping Stage
Dashpot
Rubber Coupling
Motor
Screw
Vibration Isolator

Fig.37

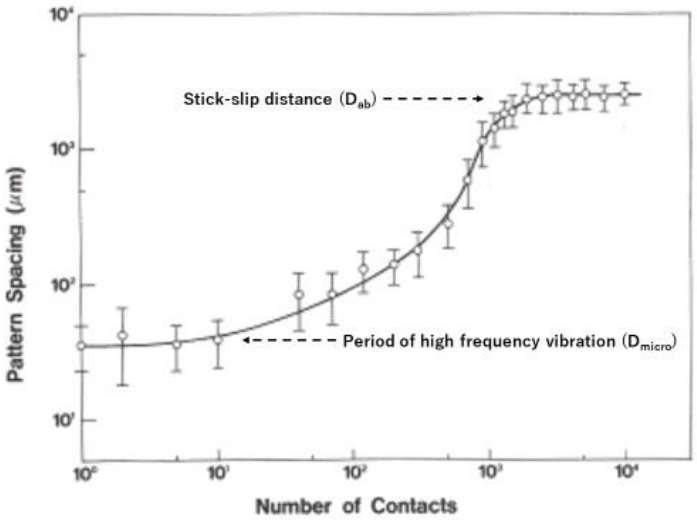
Stick-slip distance (D_{ab})
Period of high frequency vibration (D_{micro})
Pattern Spacing (μm)
Number of Contacts

Fig.38

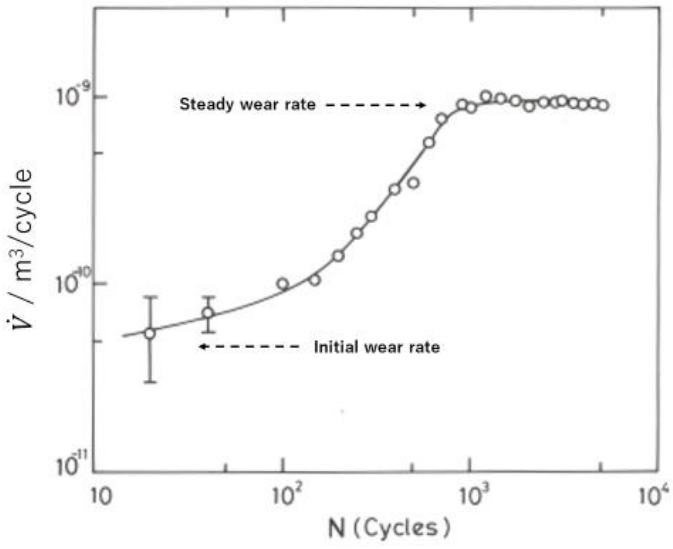
Steady wear rate
Initial wear rate
$\dot{V}$ / m^3/cycle
N (Cycles)

Fig.39

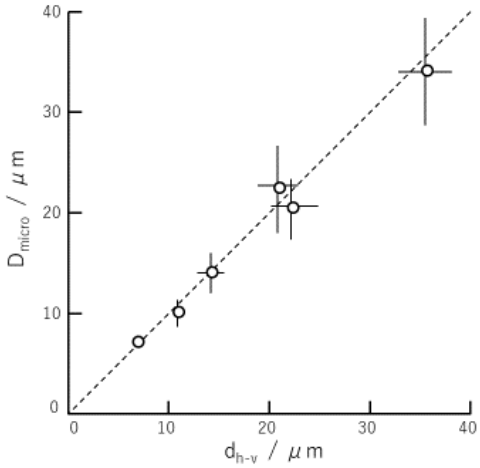
40
30
20
10
0
0
10
20
30
40
D_{micro} / μm
d_{h-v} / μm

Fig.40

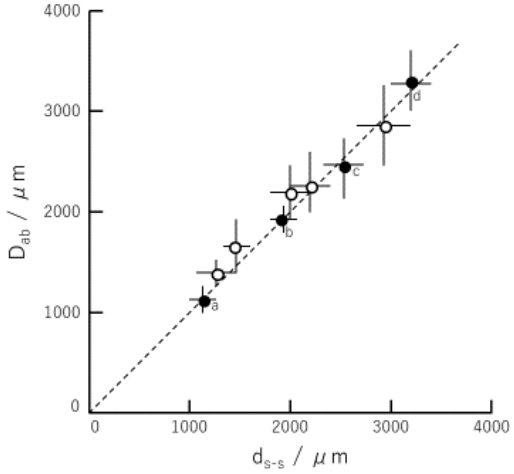
4000
3000
2000
1000
0
0
1000
2000
3000
4000
D_{ab} / μm
d_{s-s} / μm
a
b
c
d

Fig.41

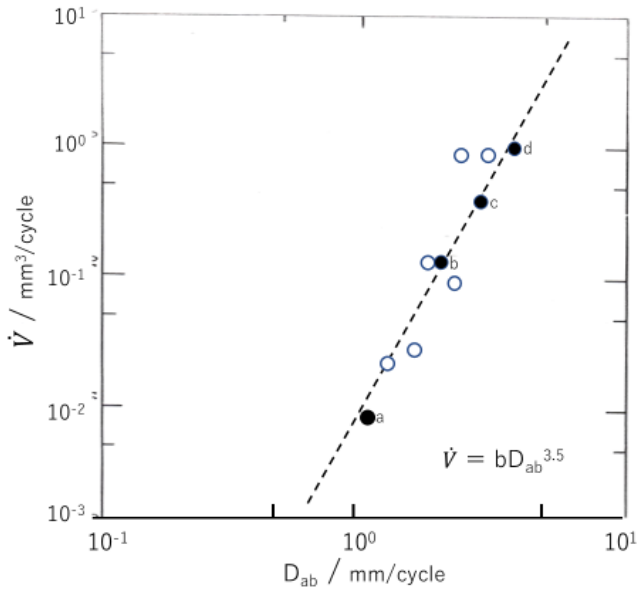
10^1
10^0
10^{-1}
10^{-2}
10^{-3}
$\dot{V}$ / mm³/cycle
a
b
c
d
$\dot{V} = bD_{ab}^{3.5}$
10^{-1}
10^0
10^1
D_{ab} / mm/cycle

Fig.42

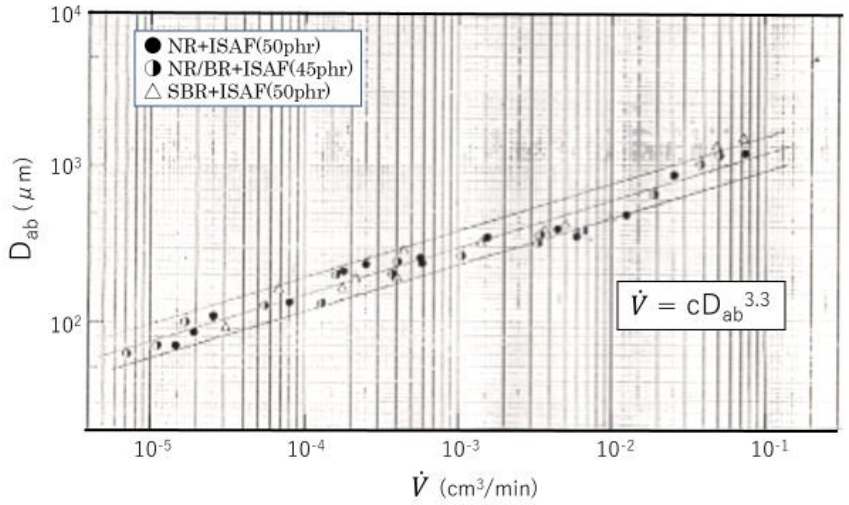
● NR+ISAF(50phr)
◑ NR/BR+ISAF(45phr)
△ SBR+ISAF(50phr)
10^4
10^3
10^2
D_{ab} (μm)
$\dot{V} = cD_{ab}^{3.3}$
10^{-5}
10^{-4}
10^{-3}
10^{-2}
10^{-1}
$\dot{V}$ (cm³/min)

Fig.43

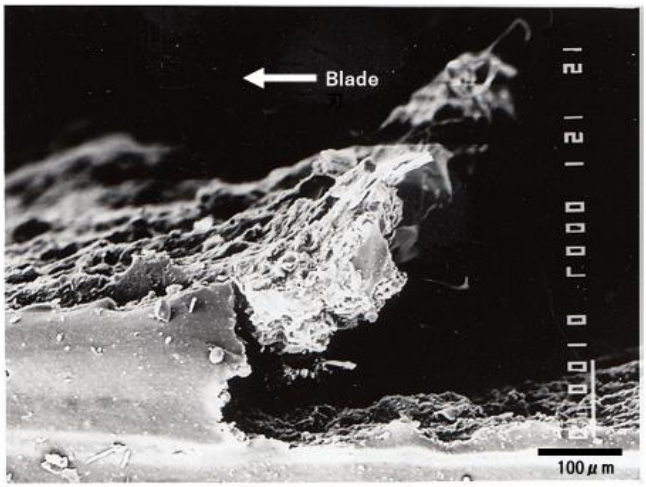

Fig.44

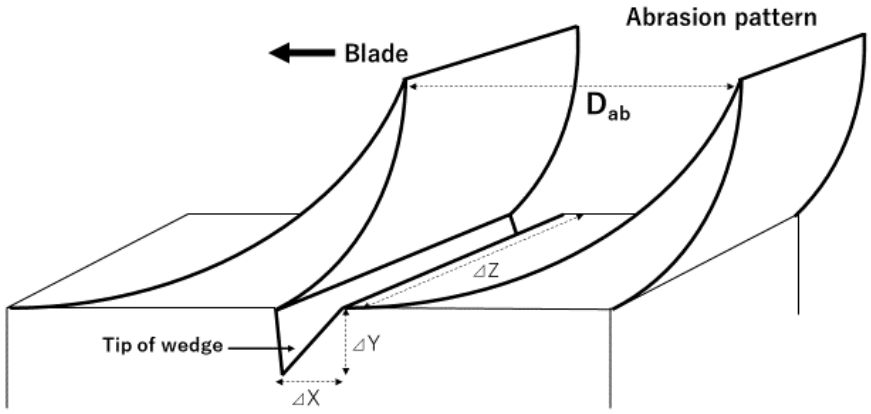

Table 1

Compound	Properties			Coefficient of friction		
	E (MPa)	tan δ	c (μm)	μ_{adh} 1.0	μ_{def} tan δ /$\sqrt{2}$	μ_{crac} $2.5\sqrt{2}(c/c_0)$
NR 1	1.21	0.07	8.0	1.0	0.05	0.21
NR 2	2.40	0.13	2.5	1.0	0.09	0.11
NR 3	4.62	0.22	1.5	1.0	0.16	0.07

Table 2

Contact time dependence		Sliding velocity dependence	
log t (sec)	n	log V (mm/sec)	1-n
$< 10^{-4}$	3/2	$> 10^{4}$	-1/2
10^{-4}～10^{-2}	1	10^{2}～10^{4}	0
10^{-2}～10^{-1}	8/10	10^{1}～10^{2}	2/10
10^{-1}～10^{1}	6/10	10^{-1}～10^{1}	4/10
10^{1}～10^{3}	2/10	10^{-3}～10^{-1}	8/10
$> 10^{3}$	0	$< 10^{-3}$	1